Polymer Chemistry

ROYAL SOCIETY OF CHEMISTRY

PAPER

View Article Online
View Journal | View Issue

Cite this: *Polym. Chem.*, 2021, **12**, 6263

Development of physical, mechanical, antibacterial and cell growth properties of poly(glycerol sebacate urethane) (PGSU) with helping of curcumin and hydroxyapatite nanoparticles†

Vafa Fakhri,[a] Aliakbar Jafari,[a] Mir Alireza Shafiei,[a] Mohammad Vahid Ehteshamfar,[b] Shima Khalighiyan,[c] Hadi Hosseini,[d] Vahabodin Goodarzi,*[e] Frederik R. Wurm,*[f] Mehrdad Moosazadeh Moghaddam[e] and Hossein Ali Khonakdar[g,h]

Received 4th August 2021,
Accepted 4th October 2021

DOI: 10.1039/d1py01040a

rsc.li/polymers

Biocompatible and antimicrobial elastomers with controlled hydrophilicity and degradation rate, as well as appropriate stiffness and elasticity, are interesting for biomedical applications, such as regenerative medicine and tissue engineering. Nevertheless, most of the tissue-engineered scaffolds do not possess a combination of the aforementioned properties. In this study, we prepare a library of poly(glycerol sebacate urethane)s (PGSU) containing different concentrations of hydroxyapatite nanoparticles (nHA) and curcumin. Poly(glycerol sebacate) prepolymers were crosslinked by hexamethylene diisocyanate, and the resulting elastomers were investigated by FTIR spectroscopy. The bioelastomers had an elastic modulus and ultimate tensile strength within a range of 1.9–4.1 MPa and 1.6–2 MPa, respectively. PGSU showed a water contact angle of 85.0 ± 2.2°. The hydrophilicity significantly improved by adding nHA, and the water contact angle was reduced to 71.8± 1.1°. It was found from the hydrolytic degradation study that while nHA accelerated the degradation rate, the hybrid nHA/curcumin compound noticeably reduced it and then increased the physiological stability of the PGSU matrix. Furthermore, the scaffolds loaded with curcumin exhibited significant antimicrobial activity against both Gram-negative (*P. aeruginosa*) and Gram-positive (*S. aureus*) bacteria. The *in vitro* biocompatibility tests showed significant cell attachment, proliferation, and viability of mouse fibroblast L929 cells. Our findings indicated that the addition of curcumin and nHA into PGSU could impart new features to the PGSU matrix and introduce the PGSU-based elastomers as a promising candidate for a range of tissue engineering applications, specifically hard tissues.

1. Introduction

With several advancements in medical science, life expectancy has increased. However, several age-related ailments, such as bone fractures and others, have also increased.[1] Biodegradable and antimicrobial polymer scaffolds can make a significant contribution to tissue engineering for the elderly, by simulating natural tissues such as bone, cartilage or tendon.[2] Here, we present a biocompatible, antimicrobial polyester elastomer with tunable hydrophilicity and biodegradability based on a composite using poly(glycerol sebacate urethane) (PGSU), curcumin, and hydroxyapatite.

For these applications, biodegradable elastomers with a crosslinked three-dimensional structure have found considerable interest because of their unique physicochemical properties like biomimetic viscoelasticity and suitable mechanical strength.[3–6] In particular, poly(glycerol sebacate) (PGS) has shown promising results in nerve,[7] cartilage,[8] skin,[9] bone,[10]

[a]*Department of Polymer Engineering, Amirkabir University of Technology, P.O. Box 15875-4413, Tehran, Iran*
[b]*Department of Mechanical Engineering, Amirkabir University of Technology, 424 Hafez Avenue, Tehran 15875-4413, Iran*
[c]*Department of Genetics, Faculty of Advanced Science and Technology, Tehran Medical Sciences, Islamic Azad University, P.O. Box: 19395-1495, Tehran, Iran*
[d]*Faculty of Engineering & Technology, University of Mazandaran, Babolsar, Iran*
[e]*Applied Biotechnology Research Center, Baqiyatallah University of Medical Sciences, P.O. Box 19945-546, Tehran, Iran. E-mail: v.goodarzi@hotmail.com, v.goodarzi@bmsu.ac.ir*
[f]*Sustainable Polymer Chemistry Group, Department of Molecules and Materials MESA+ Institute for Nanotechnology, Faculty of Science and Technology, Universiteit Twente, Enschede, The Netherlands. E-mail: f.r.wurm@utwente.nl*
[g]*Department of Processing, Iran Polymer and Petrochemical Institute, PO Box 14965/115, Tehran, Iran*
[h]*Reactive processing, Leibniz Institute of Polymer Research Dresden, Hohe Straße 6, Dresden D-01069, Germany*

†Electronic supplementary information (ESI) available. See DOI: 10.1039/d1py01040a

and cardiac[11,12] tissue engineering. PGS is a biocompatible and biodegradable polymer with a crosslinked network of random coils and hydroxyl groups joined to its backbone, and is synthesized by a polycondensation reaction between glycerol (A_3 monomer) and sebacic acid (A_2 monomer).[8,13–15] Its mechanical properties can be tailored to a certain extent by adjusting monomer ratios and synthesis conditions.[8,12,14] However, the low mechanical strength[13,14] and almost poor hydrophilicity[16,17] of PGS limit its application range for tissue engineering purposes. To overcome these issues, fillers have been added to PGS.[17–24] For instance, Gaharwar *et al.*[20] prepared nanocomposites of PGS and CNTs. It was shown that covalent crosslinks between CNTs and PGS considerably enhanced the mechanical properties. In another study, Aghajan *et al.*[18] loaded gelatin, graphene oxide, and clay nanoparticles into PGS through *in situ* polymerization. Chen *et al.*[22] studied incorporating halloysite nanotubes to modify the physical characteristics of PGS. It was shown that halloysite nanotubes could provide proper compliance and stable mechanical behavior, improve stretchability, and decrease the degradation rate. Also, Zhao *et al.*[17] fabricated a highly bioactive and degradable PGS-based elastomer containing bioactive silica glass particles (SC); it was shown that the addition of silica glass particles considerably enhanced the mechanical properties and hydrophilicity of the PGS-SC hybrid elastomers compared with PGS. In another work, Lau *et al.*[24] reported that by incorporating β-tricalcium phosphate (β-TCP) within PGS, the cross-linking degree, hydrophilicity and degradation rate, as well as cell viability, were improved significantly, making PGS/β-TCP scaffolds a promising candidate for biomedical applications.

In contrast to the direct polycondensation of glycerol and sebacic acid, which needs high temperatures and long reaction times,[9,13] several studies used isocyanate-based crosslinking of PGS prepolymers.[16,25–27] Diisocyanates react with the hydroxyl groups of the prepolymer to form crosslinked poly(glycerol sebacate urethane)s (PGSU) at lower temperatures and shorter curing times. As an example, Wu *et al.*[27] prepared (PGSU)-cellulose nanocrystal composites.

For bone tissue engineering, nano-hydroxyapatite (nHA) $[Ca_{10}(PO_4)_6(OH)_2]$, a well-known bioceramic material, is incorporated due to its biocompatibility and osteoconductive properties.[28,29] It has been widely studied in polymer/hydroxyapatite composites for biomedical applications.[19,30,31] It has been found that HDI could play the role of a coupling agent and react with hydroxyl groups on the surface of hydroxyapatite to present the hybrid inorganic–organic system with various polymers.[32,33]

An additional antibacterial property of biopolymer/nHA composites has not been reported to date. In order to keep the bio-based nature of the scaffold, we used curcumin to incorporate potential antibacterial, anti-inflammatory, antioxidant, antimicrobial, anti-proliferative, anti-infective and wound healing properties into the polymers.[34–37] Despite notable benefits, the low bioavailability of curcumin, which is due to poor aqueous solubility and low stability, limits its health advantages and medical applications.[38] One of the strategies that has been developed to address this problem is the formation of polymer–curcumin blends.[39–43] Oprea *et al.*[39] synthesized polyurethane elastomers using various molar ratios of curcumin. It was shown that the inclusion of curcumin into the backbone of the polyurethane chains resulted in enhanced thermal stability and better mechanical properties for the achieved polyurethane elastomers. In another research, Mahmood *et al.*[42] reported novel biocompatible materials for biomedical purposes by introducing curcumin blended with chitin into polyurethane.

In this study, flexible PGSU-based elastomers with different amounts of curcumin and hydroxyapatite nanoparticles (nHA) were synthesized through *in situ* polymerization. The chemical structure was investigated by Fourier transform infrared (FTIR) and proton nuclear magnetic resonance (^{1}H NMR) spectroscopy, as well as X-ray diffraction (XRD). The mechanical properties and viscoelastic behavior were investigated by quasi-static tensile and compression tests, cyclic tensile test, and dynamic mechanical-thermal analysis (DMTA). Furthermore, the morphology and elemental mapping were observed by scanning electronic microscopy (SEM) and energy dispersive X-Ray analysis (EDX). The surface wettability, as well as hydrolytic degradation, and protein adsorption of the samples were also evaluated. The release of curcumin and the antimicrobial activity of the bioelastomers were assessed to clarify further the effect of curcumin on the potential of PGSU for biomedical applications. Finally, *in vitro* biocompatibility and cell viability of the scaffolds were investigated. Altogether, the herein prepared biocompatible, biodegradable, and antimicrobial PGSU composites containing nHA and curcumin possess high potential for tissue engineering and regenerative medicine applications, and also present a promising platform technology for future *in vivo* tissue engineering studies, wherein further *in vivo* studies are needed to evaluate the effect of the synthesized bioelastomers on tissue ingrowth and tissue response.

2. Materials and methods

2.1. Materials

Glycerol (>99%), sebacic acid (99%), hydroxyapatite nanoparticles (with particle size about 100 nm), curcumin, HDI (99%), stannous 2-ethyl-hexanoate (tin(II)), 1,4-dioxane, tetrahydrofuran (≥99.0%), *N*,*N*-dimethylformamide (anhydrous, 99.8%), Dulbecco's modified Eagle medium (DMEM), penicillin–streptomycin (P/S), fetal calf serum (FCS), fetal bovine serum (FBS), sodium dodecyl sulfate (SDS) solution, bovine serum albumin (BSA), and DAPI (4′,6-diamidino-2-phenylindole) solution were purchased from Sigma-Aldrich. Phosphate buffered saline (PBS) tablets (pH 7.4) were ordered from GIBCO and bicinchoninic acid (BCA) protein assay reagent was obtained from Thermo Fisher Scientific (Pierce BCA).

2.2. Methods

2.2.1. Synthesis of the PGS pre-polymer and PGSU-based elastomers. PGSU and PGSU-nanocomposites were synthesized following the reported methods with modifications as outlined

here.[16,26,27] The PGS pre-polymer was synthesized by mixing equimolar amounts of glycerol and sebacic acid at 120 °C under a nitrogen atmosphere for 4 h. Then at the same temperature the pressure was reduced and the reaction followed for 24 h to yield a yellow resin with high viscosity. The obtained PGS pre-polymer was dissolved in 1,4-dioxane (10% w/v) for 36 h at room temperature. Afterwards, tin(II)-2-ethyl-hexanoate (0.05% w/v) was added to the solution and heated to 55 °C under constant stirring in a flask. Then, HDI, as a crosslinking agent, was added drop-wise to the solution. The reaction flask was sealed and kept at 55 °C under constant stirring for 1 h under nitrogen flow. The solution was cast onto a Teflon mold and was kept for 3 days at room temperature and then for an additional day in a vacuum oven at 30 °C to evaporate the solvent and for final curing of the samples.

For the preparation of PGSU containing nHA and curcumin, the desired amounts of nHA and curcumin were dispersed in 1,4-dioxane and ultrasonicated for 10 min. Specific amounts of the PGS pre-polymer were then dissolved in the solution and tin(II) 2-ethyl-hexanoate and HDI were added. The mixtures were cast onto Teflon molds and treated as mentioned above. The final films had a thickness of *ca.* 0.9 mm. The compositions of the prepared samples and their codes are summarized in Table 1. Also, Fig. 1a shows the photograph of the prepared samples.

2.2.2. Characterization. The molecular weight of pre-PGS was measured by gel permeation chromatography (GPC, WATERS 1515, USA). Polystyrene standards were used for the calibration. Structural analysis of the pre-PGS was carried out by proton nuclear magnetic resonance (^{1}H NMR) spectroscopy (BRUKER, DRX-500 Hz, USA). For this purpose, $CDCl_3$ was used as a solvent. Fourier transform infrared (FTIR) spectroscopy was conducted using a Bruker spectrometer (Tensor 27, Germany) in a range of 500–4000 cm^{-1} wavenumbers for the analysis of the functional groups of the PGS pre-polymer, monomers and fillers. The chemical structures of the polymeric films were characterized in attenuated total reflectance Fourier transform infrared (ATR-FTIR) mode. The crystalline structure of the synthesized PGSU-based compounds was characterized by X-ray diffractometry (XRD) utilizing a Philips diffractometer (PW1730, Netherlands) within the scanning region of 2θ = 10°–80°, at an operating voltage of 40 kV and with a Cu-K_α radiation source.

The phase structure and morphological features of the fractured-surface in liquid nitrogen were analyzed using a field emission scanning electron microscope (FESEM, MIRA3 TESCAN, Czech Republic) with the acceleration voltage of 20 kV. All samples were coated with a thin layer of gold before observation. The dispersion and distribution of the elements in the matrix were analyzed using an energy-dispersive X-ray detector (EDX, MIRA2 TESCAN, Czech Republic).

Table 1 Composition of PGSU-based samples

Sample code	Composition
PGSU	PGSU alone
PGSU-HA	PGSU + 5 wt% nHA
PGSU-Cu	PGSU + 5 wt% curcumin
PGSU-HA-Cu5	PGSU + 5 wt% curcumin + 5 wt% nHA
PGSU-HA-Cu3	PGSU + 3 wt% curcumin + 5 wt% nHA

The crosslinking density was assessed by sol–gel content analysis. First, the samples (n = 3 per condition; 10 mm diameter; 0.9–1.0 mm thickness) were weighed (W_0) and immersed in THF solvent for 48 h. The equilibrium mass (W_1) of the swollen samples was then measured. Then, the samples were dried in a vacuum oven (50 °C, 24 h), and the mass (W_2) of the fully dried samples was weighed. The sol content (ν_{sol}) and degree of swelling were calculated by eqn (1) and (2), respectively.

$$\nu_{sol}(\%) = \frac{(W_0 - W_2)}{W_0} \times 100 \quad (1)$$

$$\text{Swelling degree}(\%) = \frac{(W_1 - W_2)}{W_2} \times 100 \quad (2)$$

Quasi-static uniaxial and cyclic tensile and compression tests were carried out on the samples at room temperature following the ASTM D412 standard. Quasi-static uniaxial tensile tests were performed on the dog-bone shaped polymeric films (n = 3; 2.8 mm width; 20 mm gauge length; 0.9 ± 0.09 mm thickness) at a strain rate of 50 mm min^{-1} and a 10 N load cell till fracture using a Hounsfield H100KS testing machine (Tinius Olsen, USA), while the cyclic tensile tests were conducted under the same set-up and tensile strain rate and samples were stretched to 20% strain during 10 cycles. Quasi-static uniaxial compression tests were performed on the cylindrical punched-out samples (n = 3; 6 mm diameter; 1.4± 0.09 mm thickness) at a strain rate of 1 mm min^{-1} and up to a strain of 50%.

Dynamic mechanical thermal analysis (DMTA) was performed using a TRITEC 2000 DMA (TA Instruments) apparatus in tension mode and a temperature range of −60 to 60 °C, in the linear region with the strain amplitude of 0.02% and a heating rate of 3 °C min^{-1} on the samples with dimensions of 10 mm × 10 mm × 0.9 mm. Furthermore, multi-frequency mode (0.1, 0.5, 1, 5 and 10 Hz) was selected for systematically analyzing the viscoelastic behavior of the samples.

Surface properties and wettability of the PGSU-based elastomers were studied by measuring the water and dimethylformamide (DMF) contact angles using the sessile drop method at room temperature. For each sample, drops of DMF and distilled water of approximately 5 μL were placed on three different spots, and the mean values of measurements were reported. The images were taken after 10 seconds of contact. Also, the surface tension of the elastomers was calculated through the Owens–Wendt (eqn (3)) and the Wu harmonic mean equation (eqn (4)) methods:[44]

$$\gamma_{12} = \gamma_1 + \gamma_2 - 2\left(\sqrt{\gamma_1^d \gamma_2^d} + \sqrt{\gamma_1^p \gamma_2^p}\right) \quad (3)$$

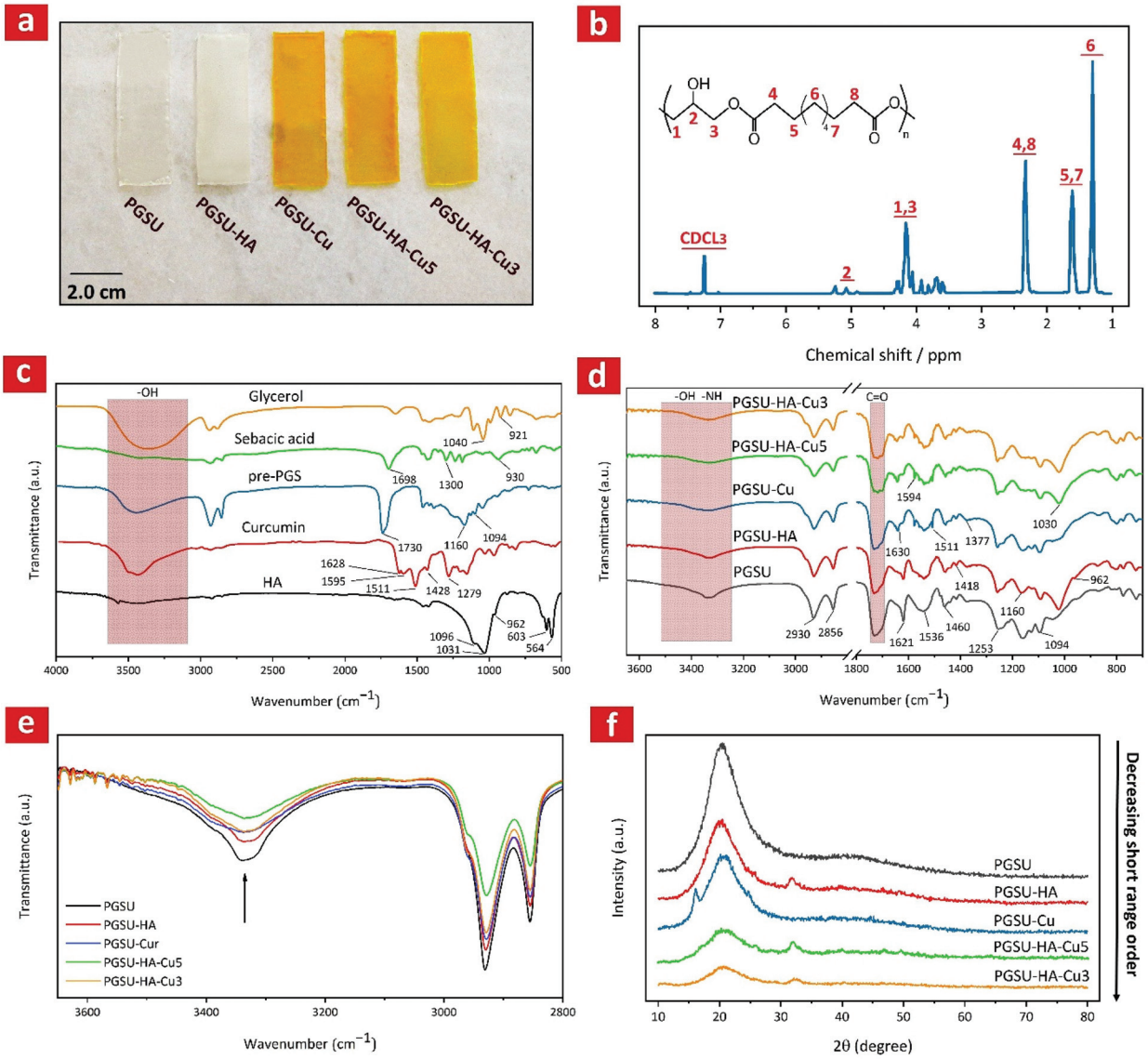

Fig. 1 (a) Photograph of the PGSU-based samples after the crosslinking process. (b) ^{1}H NMR spectrum of the synthesized pre-PGS. FTIR spectra of (c) glycerol, sebacic acid, PGS pre-polymer and fillers and (d) PGSU-based elastomers. (e) FTIR spectra of the samples; reduction in the intensity of –OH/–NH FTIR peak in the presence of nHA and curcumin supports the covalent interaction of the fillers within the PGSU network. (f) X-ray diffraction of PGSU-based samples.

$$\gamma_{12} = \gamma_1 + \gamma_2 - 4\left(\frac{\gamma_1^{d}\gamma_2^{d}}{\gamma_1^{d} + \gamma_2^{d}} + \frac{\gamma_1^{p}\gamma_2^{p}}{\gamma_1^{p} + \gamma_2^{p}}\right) \quad (4)$$

where γ_1 and γ_2 are the total surface energies of phases 1 and 2, respectively, γ_1^{d} and γ_2^{d} are the dispersive portions of the free surface energies of phases 1 and 2, and γ_1^{p} and γ_2^{p} are the polar portions. Total surface energy value for the dispersed part and polar part of water and DMF were considered 72.8, 21.8 and 51 mN m^{-1} (water) and 37.3, 32.42 and 4.88 (DMF), respectively.[45] In order to evaluate the swelling degree and analyze the hydrolytic degradation of the polymeric films, disk-shaped samples (n = 3, 8 mm in diameter and with *ca.* 0.9 mm thickness) were immersed in lipase-containing PBS solution (enzyme concentration: 110 U L^{-1}) at pH 7.4 and 37 °C. For the swelling study, the polymeric films were collected after 24 h, and the excess surface liquid was gently drained with filter paper. The swelling ratio was calculated according to eqn (2). For the degradation study, the weight loss during the degradation (30 days was considered as hydrolytic degradation time in this study) was recorded at a predetermined time (5-day periods). The degree of hydrolytic degradation was calculated from eqn (5):

$$\text{Degradation}(\%) = \frac{(W_i - W_d)}{W_i} \times 100 \quad (5)$$

where W_i is the initial weight of the sample, and W_d is the weight of the residual dried sample at each time.

To determine the *in vitro* release rates of curcumin, first, the standard curve was prepared using a UV-Vis spectrophotometer (LAMBDA 365, PerkinElmer, USA) at 425 nm and curcumin solution with concentrations of 5, 10, 20, 40, and 60 μM. Then the curcumin concentration in PBS solution during the hydrolytic degradation was calculated using the calibration curve ($y = 257.32x + 24.87$, correlation coefficient $R = 0.9983$) at predetermined time intervals (1, 3, 6, 9, 15, 21, and 27 days).

2.2.3. Protein adsorption. Protein adsorption on the bioelastomer surface was determined by washing the disk-shaped samples (6 mm diameter) twice with PBS before immersing in 10% fetal bovine serum (FBS) for 24 h at 37 °C. In order to remove non-specifically adsorbed proteins, the samples were washed three times with PBS. Afterward, samples were subjected to 2% sodium dodecyl sulfate (SDS) solution with shaking (50 rpm, 37 °C) for 6 h to collect the adhered proteins. The supernatant was collected and protein concentration was quantified using the bicinchoninic acid (BCA) protein assay reagent. In brief, equal amounts of the collected supernatant and the protein assay reagent were incubated at 37 °C for 2 h, and then the supernatant was quantified using a UV-Vis spectrophotometer (LAMBDA 365, PerkinElmer, USA) at 562 nm. Bovine serum albumin (BSA) was used as a standard.

2.2.4. Antibacterial activity. Agar diffusion method was utilized to assess the antimicrobial activity of the synthesized samples against *S. aureus* and *P. aeruginosa*. The samples were cut into discs with a diameter of 10 mm and sterilized under UV light exposure for 20 min on both sides. Then, the polymer discs were placed on agar plate Petri dishes containing bacterial strains. The Petri dishes were incubated at 37 °C for 24 h. After that, the bacterial growth inhibition zone around the examined samples was measured.

2.2.5. *In vitro* biocompatibility and cell culture experiments. *In vitro* biocompatibility was assessed by studying the L929 cell (mouse fibroblast cell line from the Stem Cell Technology Research Center, Pasteur Institute, Iran) proliferation on the surface of the nanocomposite. The cells were incubated for growing in Dulbecco's modified Eagle medium (DMEM supplemented with 10% fetal calf serum (FCS) and 1% penicillin/streptomycin) under standard incubation conditions (37 °C, 5% CO_2, 95% relative humidity). The cells were cultured until 75% confluence, and then they were trypsinized and ready for seeding on the nanocomposites. Before the seeding process, the PGSU nanocomposites (diameter = 10 mm, thickness ~1 mm, in triplicates for each concentration) were sterilized by UV light exposure for 20 min on both sides and then put in a 24-well plate. L929 cells were initially seeded on the polymer surface at a density of 3×10^4 cell per sample and the culture media was changed every two days. Cell viability was evaluated by the 3-(4,5-dimethylthiazol-2-yl)-2,5-diphenyltetrazolium bromide (MTT) assay. At predetermined culture times (1, 3, 5, and 7 days), each well was treated with MTT solution and incubated under standard conditions (for 4 h at 37 °C) for formazan crystal formation, followed by dissolving in dimethyl sulfoxide (DMSO). The absorbance of the solution was evaluated at 570 nm using a microplate reader (Spectra Max M5e). Tissue culture polystyrene (TCPS) surface was used as a positive control. A scanning electron microscope (FESEM, MIRA3 TESCAN, Czech Republic) was used to observe the morphologies of the cells cultured on the samples for 3 days.

Nuclear staining with DAPI (4′,6-diamidino-2-phenylindole) was conducted to further evaluate the L929 cell adherence and proliferation on the bioelastomers under fluorescence microscopy (Nikon Eclipse TE-2000U). For this purpose, the seeded cells were fixed with 4% paraformaldehyde (4 °C, 30 min) on days 1 and 5 after cell seeding and stained with DAPI solution.

2.3. Statistical analysis

The experimental results were represented as mean ± SD (standard deviation); all data were generated from three independent experiments. Statistical analysis was conducted using one-way ANOVA followed by Tukey's *post-hoc* analysis. Statistical significance was represented as $*p < 0.05$, $**p < 0.01$, $***p < 0.001$.

3. Results and discussion

3.1. Physicochemical structure of PGSU and PGSU composites

Gel permeation chromatography (GPC) showed that the pre-PGS used in this study had a number average molecular weight (M_n), weight average molecular weight (M_w), and polydispersity index (PDI) of 1530 g mol^{-1}, 10 460 g mol^{-1} and 6.8, respectively.

The successful synthesis of pre-PGS was characterized by proton-NMR spectroscopy. As shown in Fig. 1b, peaks attributed to the sebacic acid part were identified at δ = 1.3 ppm (No. 6), δ = 1.61 ppm (No. 5 and 7), and δ = 2.34 ppm (No. 4 and 8), while peaks at δ = 4.05–4.35 ppm (No. 1 and 3) and δ = 4.96–5.23 ppm (No. 2) were assigned to the glycerol part.

The chemical structures of the raw materials and synthesized PGSU-based elastomers were determined from the FT-IR spectra shown in Fig. 1. Fig. 1c shows the FTIR spectra of nHA and curcumin, as well as of the PGS pre-polymer and its monomers. Curcumin showed its characteristic peaks at 1279 cm^{-1} (aromatic C–O stretching vibrations), 1428 cm^{-1} (olefinic C–H bending vibrations), 1511 cm^{-1} (C═O and C–C vibrations), 1595 cm^{-1} (stretching vibration of phenyl rings), and 1628 cm^{-1} (C═O and C═C mixed stretching vibration) as well as a broad peak at 3110–3640 cm^{-1} (phenolic O–H stretching vibration), as have been reported in other studies in the literature.[39,41,46] HA nanoparticles showed absorption bands at 564 cm^{-1} and 603 cm^{-1} corresponding to the ν4 bending vibrations of P–O–P, a weak peak at 962 cm^{-1} assigned to the ν1 symmetric P–O stretching vibrations, strong absorption bands at 1031 cm^{-1} and 1096 cm^{-1} attributed to the P–O stretching vibrations of PO_4^{3-}, a broad absorption band at 3230–3510 cm^{-1} corresponding to stretching vibration of O–H and a weak peak at 3575 cm^{-1} ascribed to the vibrations of

OH^- ions in the hydroxyapatite crystal lattice.[28,47] Also, the absorption bands at 921 cm^{-1} and 3000–3650 cm^{-1} appearing in the spectrum of glycerol are attributed to the bending and stretching vibrations of hydroxyl groups (–OH), respectively, while the peak at 1040 cm^{-1} is assigned to ether groups (C–O stretching). Sebacic acid showed characteristic peaks at 930 cm^{-1}, 1300 cm^{-1}, and 1698 cm^{-1} which were assigned to hydroxyl groups (O–H bending), ether groups (C–O stretching), and C═O carbonyl groups (C═O stretching), respectively.

The primary characteristic of PGS is the reaction between hydroxyl groups of glycerol and carboxyl groups of sebacic acid that leads to the formation of the ester linkage, which is confirmed by FTIR with a peak at 1730 cm^{-1} for the ester carbonyl band (C═O stretching vibration) and obvious peaks at about 1160 cm^{-1} and 1094 cm^{-1} for C–O, indicating the successful synthesis of pre-PGS; furthermore, the broad peak appearing at 3460 cm^{-1} is associated with the stretching vibrations of free hydroxyl groups in the PGS pre-polymer structure.[9,18,19,26,48]

Fig. 1d shows the FTIR spectra of PGSU-based samples. It can be seen from the spectrum of pure PGSU that with the addition of HDI as a crosslinker, the peak corresponding to the vibration of the free hydroxyl groups of the PGS pre-polymer shifted to 3333 cm^{-1} which is attributed to the overlapping of unreacted hydroxyl groups (–OH stretching vibration) in PGS and –NH stretching vibration bands in urethane groups.[26,32] This shift indicates the increase in the hydrogen bonding forces in the system by adding HDI.[48]

The absorption bands of amide I (C═O stretching), amide II (N–H and C–H), and amide III (C–N stretching) can be seen at 1621 cm^{-1}, 1536 cm^{-1}, and 1253 cm^{-1}, respectively.[25–27,32] The wavenumber range of 1800–2800 cm^{-1} was ignored from the presented spectra in Fig. 1d because the studied samples did not show any characteristic absorption peak in the neglected wavenumber range. The absence of the characteristic isocyanate group band (–N═C═O) at 2270 cm^{-1} indicates the complete consumption of the HDI during the course of the curing reaction for all the samples.[26,39,41]

Hence, a noticeable intensity reduction of the –OH stretching vibration, disappearance of the isocyanate group band at 2270 cm^{-1}, as well as the presence of amide groups and N–H absorption bands confirmed the successful chemical crosslinking by HDI and formation of urethane linkages due to the reaction between HDI and hydroxyl groups of pre-PGS.

The presence of curcumin in the samples (PGSU-Cu, PGSU-HA-Cu3, PGSU-HA-Cu5) was confirmed by the emergence of three new peaks at 1630 cm^{-1}, 1594 cm^{-1}, and 1511 cm^{-1}. On the other hand, the strong absorption peak at 1030 cm^{-1} and the weak peak at 962 cm^{-1} authenticate the presence of nHA in PGSU-HA, PGSU-HA-Cu3, and PGSU-HA-Cu5. The absorption bands at 2930 cm^{-1}, 2856 cm^{-1}, respectively, are attributed to asymmetric and symmetric $-CH_2$ stretching vibration of PGS, which overlapped with the absorption bands corresponding to the $-CH_2$ group of HDI and curcumin; absorbance peaks at 1460 cm^{-1}, 1418 cm^{-1}, and 1377 cm^{-1} are attributed to other modes of $-CH_2$ group and methyl group ($-CH_3$) deformations.[9,18,19,41] The FTIR spectrum of PGSU composites showed a noticeable difference in the intensity and pattern of absorption bands at 1710–1730 cm^{-1} (ester carbonyl band) and 1160 cm^{-1} (C–O), indicating the influence of nHA and curcumin on the chemical structure of the ester groups; the broadness of the C═O peak can also be attributed to the overlapping of a free C═O stretch with a hydrogen-bonded C═O.

By adding nHA or curcumin to PGSU, hydroxyl groups showed lower intensity, implying the reaction of functional groups of curcumin and nHA with other active groups, as well as an increase in the number of intermolecular and intramolecular hydrogen bonding between components, *i.e.*, indicating that the consumption of free hydroxyl groups belongs to PGS, nHA, and curcumin, presumably due to the formation of urethane linkage between PGS and nHA or PGS and curcumin (see Fig. 1e and Fig. 2).

Crystal structures of the PGSU-based elastomers were analyzed using XRD at room temperature, and the obtained XRD patterns are exhibited in Fig. 1f. All compounds showed a broad peak at about $2\theta = 20°$ attributed to Miller indices (110), the characteristic diffraction pattern of amorphous polymers,[10,18,49] indicating that all the samples have an amorphous structure. The intensity of the aforementioned peak was reduced with incorporation of nHA as well as curcumin within the PGSU matrix; this reduction was more pronounced for the hybrid nHA–curcumin system. This behavior leads to the conclusion that nHA, curcumin and their hybrid composites can noticeably influence the short-range order microstructural phases of the amorphous PGSU matrix. XRD patterns of pure curcumin and nHA are exhibited in Fig. S1.† The peak at 31.7° for sample of PGSU-HA was indexed to the (211) plane, indicates the presence of nHA. As well, the curcumin characteristic peak was detected at $2\theta = 16.2°$ for PGSU-Cu; this diffraction peak was disappeared for the XRD patterns of the hybrid composites and simultaneously, the intensity of the main characteristic peak of PGSU matrix ($2\theta = 20°$) reduced significantly. It can probably be due to the disorder of the short-range regular structure of PGSU chains and the formation of an amorphous complex as a result of intermolecular or intramolecular interactions that may be occurred between nHA and curcumin.

3.2. Morphology

Fig. 3 shows the SEM images from the cross-sectional fractured surfaces of the PGSU composites containing nHA. In Fig. 3, the distribution of components in the PGSU matrix is shown at three different magnifications. PGSU-HA exhibited agglomeration and more particles in images compared to the hybrid samples even though all the composites had the same nHA percentage, implying that the presence of curcumin in the matrix leads to better dispersion of nHA. It could probably be due to the increment of the potential to form intermolecular and intramolecular hydrogen bonds in the compound since curcumin imparts more hydroxyl groups to the system. On the other hand, the simultaneous presence of curcumin and nHA in the system disrupts the short-range order structure of the

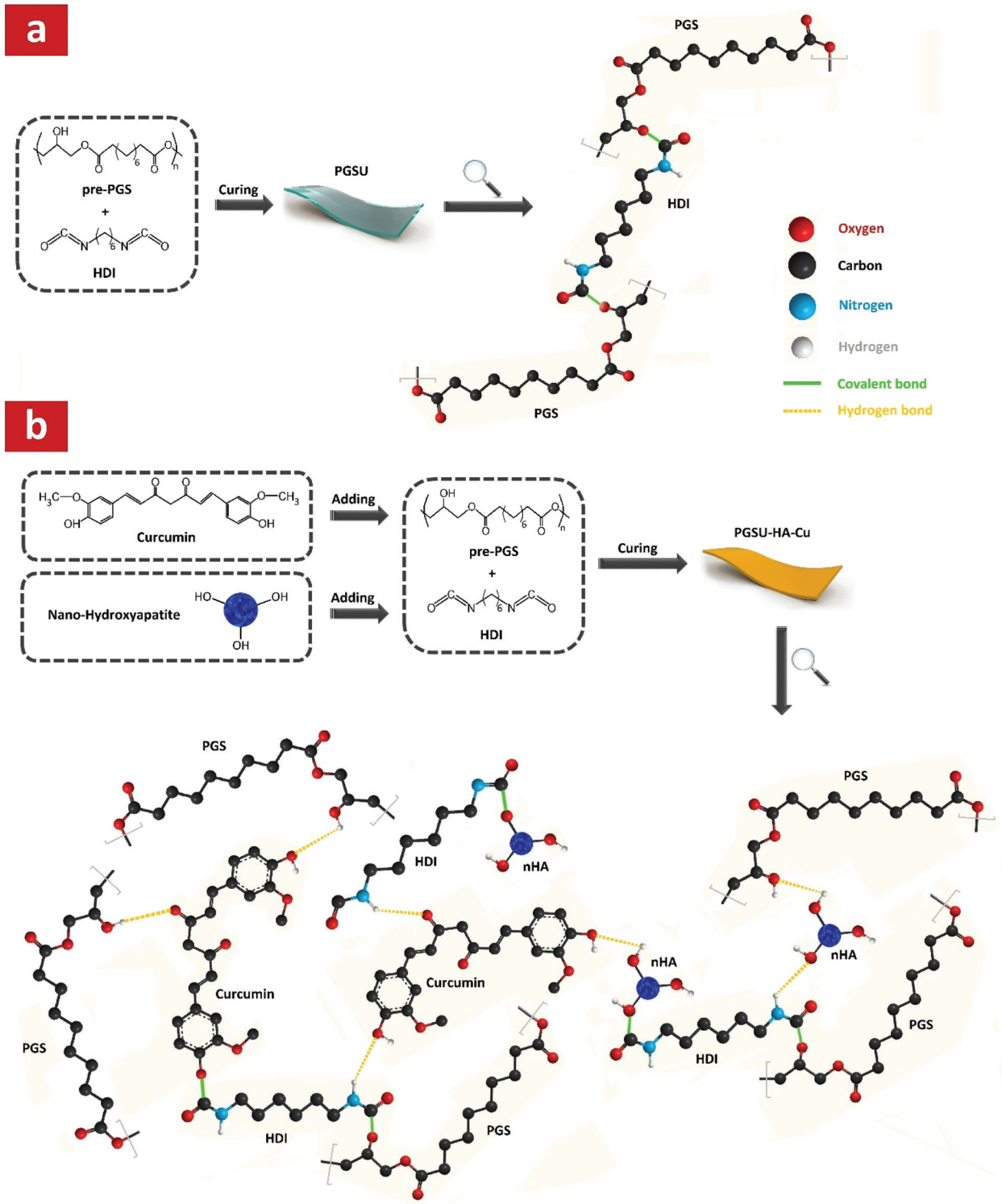

Fig. 2 Scheme of the possible reactions of PGSU-based elastomers during the crosslinking process, (a) within the PGSU structure and (b) within the PGSU-HA-Cu structure.

PGSU matrix, which may improve the dispersion of the fillers (see Fig. 1f).

Interestingly, PGSU-HA-Cu3 showed more broken agglomerates and further uniform dispersion of fillers in the PGSU matrix compared to PGSU-HA-Cu5. This behavior may be due to two probable reasons. First, the lower curcumin content in PGSU-HA-Cu3 than in PGSU-HA-Cu5 may lead to better dispersion of curcumin in the PGSU-HA-Cu3 sample, which can

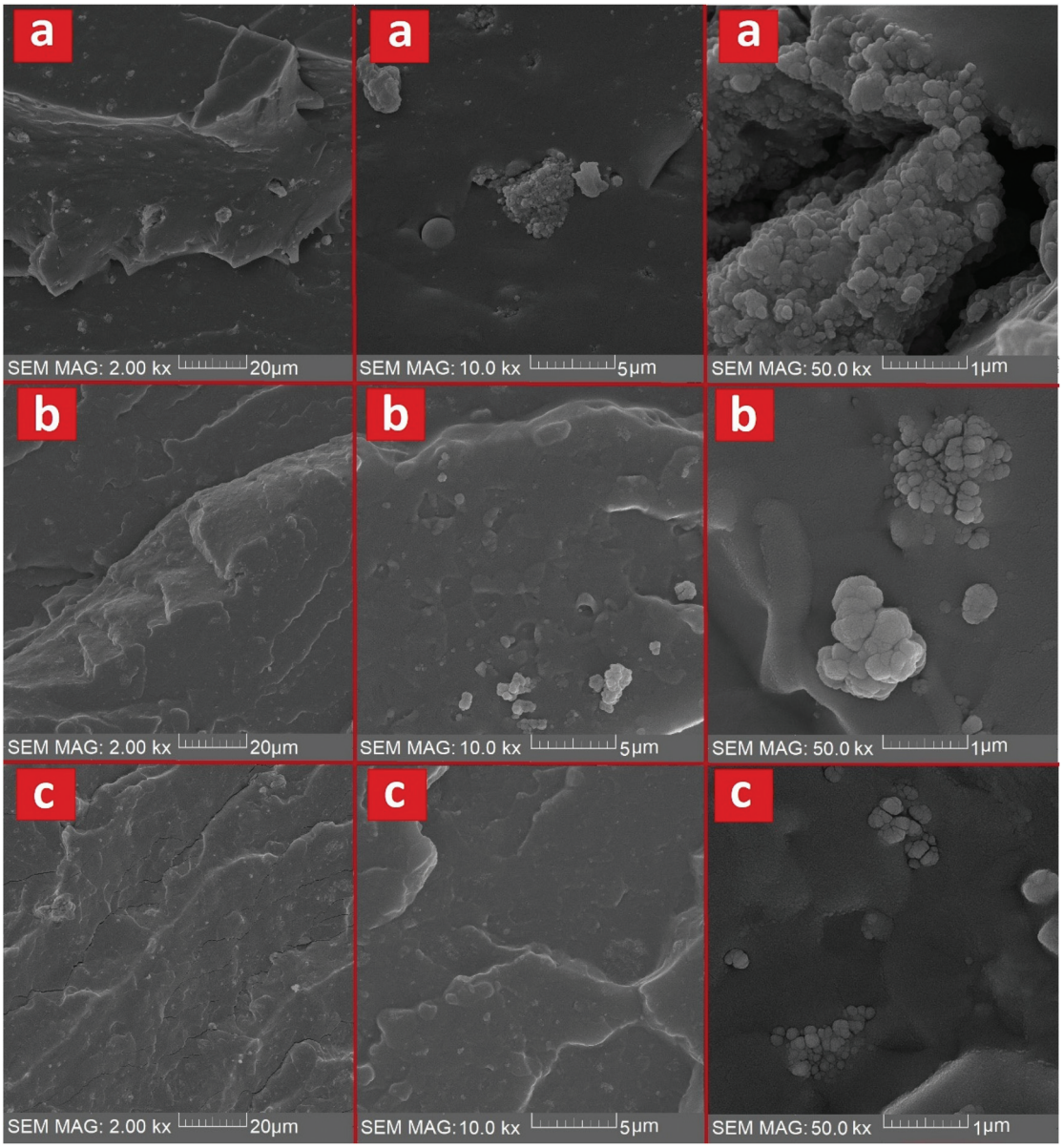

Fig. 3 Fracture surface morphologies of PGSU nanocomposites at three different magnifications, (a) PGSU-HA, (b) PGSU-HA-Cu5, (c) PGSU-HA-Cu3.

improve interactions between the curcumin moieties and nHA. Second, the higher disorder in the short-range regular structure of PGSU-HA-Cu3 than PGSU-HA-Cu5 (Fig. 1f) may facilitate dispersion of the fillers in the polymeric matrix.

Energy-dispersive X-ray spectroscopy (EDX) was used as a complementary technique for further morphological investigation as well as elemental mapping, and its results are presented in Fig. 4. The EDX spectra proved the presence of phosphorus (P) and calcium (Ca) in the nHA-containing samples. In particular, in the PGSU-HA-Cu3 and PGSU-HA-Cu5 samples, a well-distributed signal of Ca and P within the PGSU matrix was detected, which is in good agreement with the SEM images. This behavior could be attributed to the stabilization of nHA by curcumin *via* hydrogen bonds and covalent bonds resulting in better dispersion of nHA in the polymer matrix. Moreover, the ratio of Ca to P for PGSU-HA, PGSU-HA-Cu5 and PGSU-HA-Cu3 was found to be about 1.87, 1.76 and 1.80 respectively, which is close to the stoichiometric Ca/P value of hydroxyapatite (1.67).

3.3. Swelling behavior, mechanical properties, and crosslinking density

One of the methods to assess the possible covalent crosslinking formed between PGSU and the fillers is to evaluate the change in crosslinking density due to the addition of nHA and curcumin. The swelling method was used to determine the crosslinking density of the samples by evaluating the amount of sol and gel contents. Fig. 5a shows the general appearance

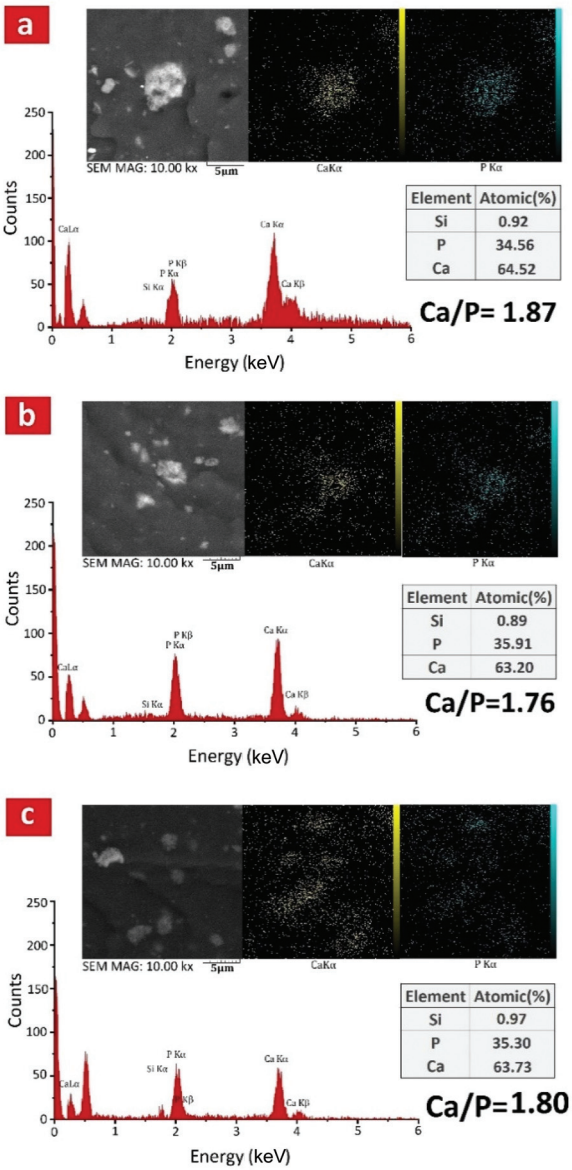

Fig. 4 EDX spectra and mapping of Ca and P for the PGSU nanocomposites, (a) PGSU-HA, (b) PGSU-HA-Cu5, and (c) PGSU-HA-Cu3.

of the samples before and after swelling in THF. As can be seen, all the samples expanded and almost doubled their original size after soaking. The swelling degree of the samples calculated by eqn (2) is presented in Fig. 5b and Table 2. Clearly, by adding fillers to the PGSU network, the solvent uptake decreased, implying that nHA and curcumin have participated in the formation of polymer networks and present new crosslinking sites for the PGSU chains (Fig. 2). Also, in accordance with observed swelling behavior, the incorporation of nHA and curcumin remarkably decreased the amount of sol content probably due to the formation of covalent bonds between the fillers and PGSU (Fig. 5c). Interestingly, although adding nHA and curcumin reduced the sol content, their simultaneous incorporation significantly intensified the reduction of sol content, showing the outstanding synergistic effect of nHA and curcumin.

Mechanical properties of the PGSU-based elastomers were assessed by uniaxial tensile testing (Fig. 5d and Table 2). For elastomers, the crosslinking density (n) can be calculated by the rubber elasticity model using E through eqn (5):[48]

$$E = 3RTn \quad (5)$$

where T is the temperature and R is the universal gas constant. According to the crosslinking density calculated based on the rubber elasticity theory, the number of crosslinks in the PGSU-based elastomers ranged from 266.5 ± 5.6 mol m^{-3} for the pure PGSU and increasing up to 549.2 ± 11.2 mol m^{-3} for the PGSU-HA-Cu5 nanocomposite (Table 2). This observation is consistent with the FTIR analysis results (Fig. 1d and e) and swelling behavior (Fig. 5b and c). PGSU-Cu presented a crosslinking density of 445.5 ± 14.9 mol m^{-3}, more than one and half-fold higher than PGSU, while PGSU-HA showed a crosslinking density of 340.5 ± 18.6 mol m^{-3}. One could infer that curcumin has a higher impact on crosslinking density and mechanical properties of PGSU in comparison with nHA. With the increase of the crosslinking degree, Young's modulus (E) of the elastomers showed a remarkable ascending trend, while there was no regularity in the change of the ultimate tensile strength (UTS) (Fig. 5e and Table 2). Meanwhile, the elongation at break of the samples exhibited significant descending trend, reducing from 125.2 ± 4.2% (PGSU) to 66.0 ± 5.7 (PGSU-HA-Cu5) (Fig. 5f). A decrease in the elongation at break was expected because of an increase in the crosslinking density with the addition of fillers. For the hybrid samples, simultaneously incorporating nHA and curcumin presented higher Young's modulus compared to other samples; Young's modulus of the PGSU elastomer was 1.98 ± 0.03 MPa, and the addition of nHA-curcumin (PGSU-HA-Cu5) resulted in a more than two-fold increase in the elastic modulus, up to 4.08 ± 0.06 MPa. The improvement of mechanical performance probably was due to the reinforcement effect of the high stiff inorganic hydroxyapatite mineral phase and rigid structure of curcumin, as well as the formation of the covalent bonds and increasing hydrogen bonding between the fillers and the PGSU backbone, as previously reported in the literature for elastomeric nanocomposites containing various fillers such as CNT,[20,49] silica bioactive glass,[17] graphene flakes,[50] curcumin,[39,43] and hydroxyapatite.[51]

Moreover, the fracture surface of the samples during uniaxial tensile testing was analyzed by SEM technique for a more in-depth investigation on the effect of fillers on PGSU's mechanical properties and the polymer chain network (Fig. 5g). The fractured surface of the PGSU shows the formation of force concentration spots which with increasing stress ultimately causes failure, indicative of a ductile fracture. Adding nHA lowered the surface deformation, and for PGSU-Cu, PGSU-HA-Cu3, and PGSU-HA-Cu5, minimum surface deformation was observed. Typical surface morphology of a brittle fracture can be seen for the samples with higher

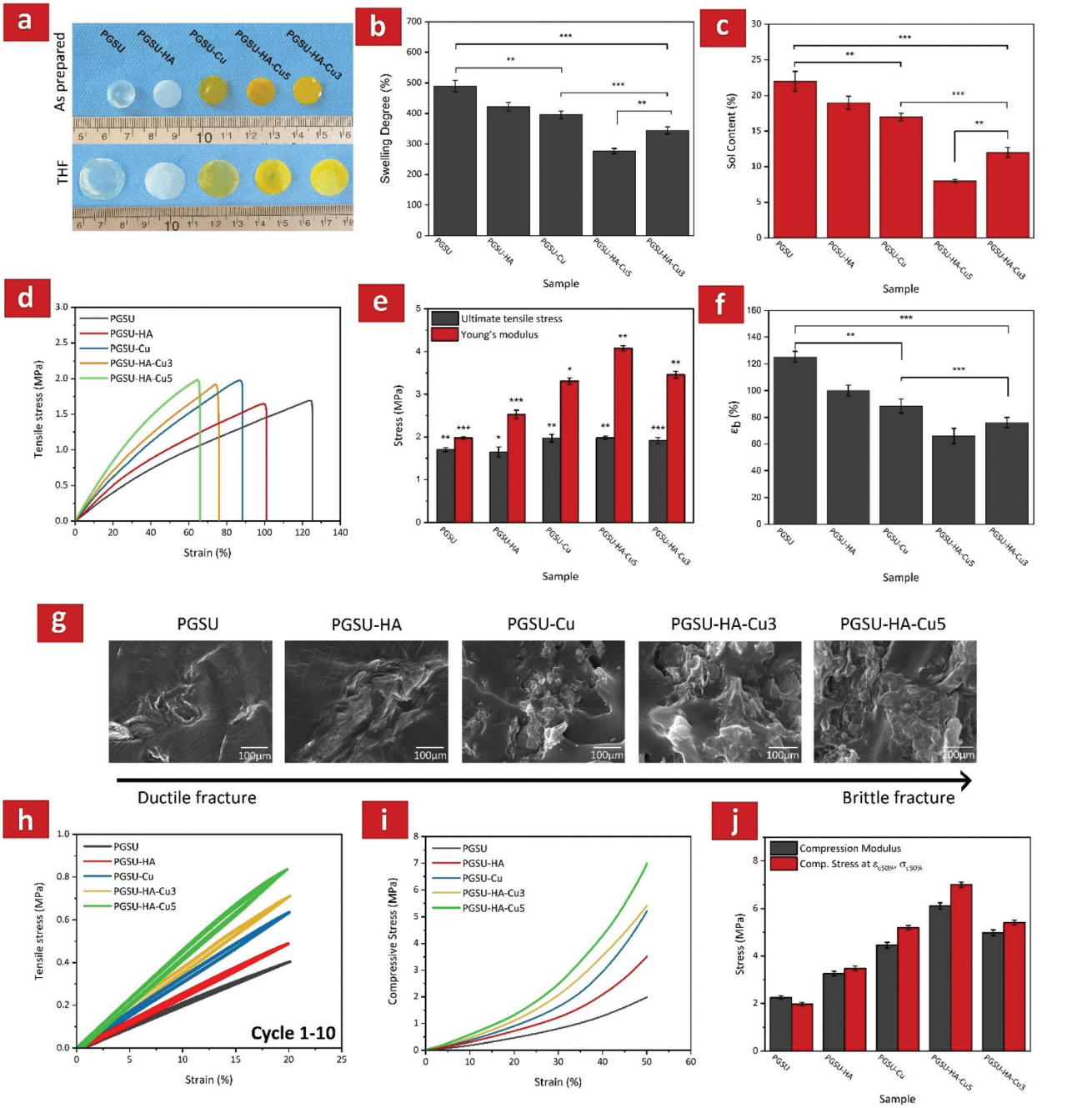

Fig. 5 (a) PGSU-based samples before and after swelling in THF. (b) Swelling degree and (c) calculated sol-content of the samples. (d) Quasi-static tensile stress–strain curves, (e) Young's modulus and ultimate tensile strength, and (f) elongation at break of the PGSU-based elastomers. (g) SEM images of fractured surfaces of the samples after tensile testing. (h) Cyclic tensile stress–strain curves (i) Quasi-static compression stress–strain (test terminated at a compressive strain of 50%) curves, and (j) compression modulus and compressive stress of the synthesized bio-elastomers. (Statistical significance was shown as $*p < 0.05$, $**p < 0.01$, $***p < 0.001$, $n = 3$).

crosslinking density, proving the results acquired by mechanical testing.

The efficiency of the PGSU-based bioelastomers to engineer elastomeric tissues which come under pulsating or frequent *in vivo* mechanical forces was studied by assessing the mechanical properties of the samples under cyclic tensile conditions (Fig. 5h). As observed from the quasi-static uniaxial tensile test, all the bioelastomers demonstrate a linear stress–strain curve until 20% strain. The samples were subjected to 20% cyclic tensile strain, and the loading and unloading stress–strain curve for 10 continuous cycles was monitored. Obviously, all the samples showed highly elastomeric characteristic with almost minimal hysteresis loop during loading. The amount of hysteresis (e_d) during the cyclic tensile test was

Table 2 Mechanical properties and degree of crosslinking for PGSU-based samples

Sample	Swelling degree (%)	Sol content (%)	E (MPa)	UTS (MPa)	ε_b (%)	n (mol m^{-3})	Compression modulus (MPa)	Comp. stress at $\varepsilon_{c50\%}$, $\sigma_{c50\%}$ (MPa)
PGSU	560 ± 22	22 ± 1.4	1.98 ± 0.03	1.70 ± 0.05	125.2 ± 4.2	266.5 ± 5.6	2.25 ± 0.08	1.97 ± 0.08
PGSU-HA	483 ± 16	19 ± 0.9	2.53 ± 0.10	1.65 ± 0.12	100.1 ± 4.1	340.5 ± 18.6	3.26 ± 0.10	3.48 ± 0.10
PGSU-Cu	452 ± 15	17 ± 0.5	3.31 ± 0.08	1.97 ± 0.09	88.4 ± 5.3	445.5 ± 14.9	4.46 ± 0.12	5.20 ± 0.09
PGSU-HA-Cu5	316 ± 10	8 ± 0.2	4.08 ± 0.06	1.98 ± 0.04	66.0 ± 5.7	549.2 ± 11.2	6.11 ± 0.13	7.00 ± 0.11
PGSU-HA-Cu3	394 ± 13	12 ± 0.7	3.46 ± 0.08	1.92 ± 0.07	76.1 ± 3.8	465.7 ± 15.0	4.98 ± 0.12	5.41 ± 0.10

n – Cross-linking density; E – Young's modulus from quasi-static tensile stress–strain curves; UTS – ultimate tensile strength; ε_b – Elongation at break.

determined using the area between the loading and unloading curves. The hysteresis ratio (h_r) was determined using the following equation:[25,26]

$$h_r = \frac{e_0 - e_r}{e_0} = \frac{e_d}{e_0}$$

where e_0 is the input strain-energy density (area below the loading curves), and e_r is the retraction strain-energy density (area below the unloading curves). Under cyclic tensile testing, PGSU, PGSU-HA, and PGSU-Cu were characterized by a negligible low h_r of 0.04, 0.05, and 0.07, respectively. Simultaneous incorporation of nHA and curcumin increased the amount of hysteresis, where PGSU-HA-Cu3 and PGSU-HA-Cu5 after 10 cycles showed a h_r of 0.9 and 0.11, respectively. At least a part of the increase in hysteresis for the hybrid networks (PGSU-HA-Cu) presumably could be due to the increment of heterogeneity of the crosslinked network, which is consistent with the DMTA results, discussing in detail in section 3.4 (dynamic mechanical thermal analysis).

The compressive properties of the bioelastomers were studied using quasi-static compression testing (Fig. 5(i and j)) and compression modulus and the compressive stress at 50% strain ($\sigma_{c50\%}$) were determined, as tabulated in Table 2. As expected, with adding fillers, the compressive modulus increased, where the compressive modulus changed from 2.25 ± 0.08 MPa for pure PGSU to 6.11 ± 0.13 MPa for PGSU-HA-Cu5, indicating that adding nHA and curcumin results in stiffer constructs. None of the samples exhibited structure collapse or fracture since the fracture strain was not observed for any of them; all bioelastomers showed a highly elastomeric network that could withstand compressive strain up to 50%.

The mechanical tests indicate that by incorporation of nHA and curcumin, PGSU can be tailored to reach a range of mechanical properties (Young's modulus from ≈1.9 to 4.2 MPa and compression modulus from 2.2 to 6.2 MPa), mimicking the mechanical properties of various tissues.

3.4. Dynamic mechanical thermal analysis

As shown earlier, the reaction between the fillers and PGSU chain backbone and consequently the increase in the degree of crosslinking can significantly influence the elasticity and strength of the synthesized bioelastomers and affect their performance, particularly for applications in which load-bearing is essential. To further understand the impact of the fillers on the PGSU chain network and determine the glass transition temperature and viscoelastic behavior, dynamic-mechanical analysis was conducted at a constant frequency of 1 Hz during the temperature sweep.

It can be observed from Fig. 6a that in the glassy region, the storage modulus (E') of the PGSU composites was larger than that of pure PGSU. There are two reasons to explain this behavior: first, the rigid nature and stiffening effect of curcumin and nHA particles can improve the load-bearing capacity of the PGSU matrix.[39,52] The formation of hydrogen bonds and covalent bonds between the fillers and the PGSU matrix and increasing crosslinking density lead to an improvement in the interfacial binding force and restriction of the movement of the PGSU chains.

Fig. 6(b) and (c) demonstrate the temperature dependency of loss modulus (E'') and loss factor ($\tan\delta$) from −60 °C to 60 °C, respectively. It can be found that the loss modulus values of the PGSU-based elastomers were over one order of magnitude lower than the corresponding storage modulus values, implying that the bulk response of the samples to an applied deformation is mainly elastic. The temperature corresponding to the maximum value of $\tan(\delta)$ is usually considered the glass transition temperature (T_g) of polymers. While it can be proximate to T_g, it should be noted that the temperature for $\tan(\delta)_{max}$ is much more sensitive to parameters such as crosslinking density, filler content, or blend morphology than T_g itself; actually, it is the maximum in the loss modulus (E''), which is very close to T_g.[53] The glass transition temperatures determined from the peaks of $\tan\delta$ and E'' are listed in Table 3. All the samples exhibited low glass transition temperatures (remarkably below room temperature), suggesting a highly elastomeric mechanical behavior of the PGSU-based elastomers at body temperature, *i.e.*, under physiological conditions.

As evident in Fig. 6b, pure PGSU exhibits a loss modulus peak at −9.5 °C, corresponding to its glass transition temperature. For PGSU-Cu, despite higher crosslinking density than PGSU, the reduction in T_g could probably be a reflection of an increase in free volume fraction in the network due to the presence of curcumin, which facilitates the free movement of polymeric chains. Meanwhile, the addition of nHA barely influ-

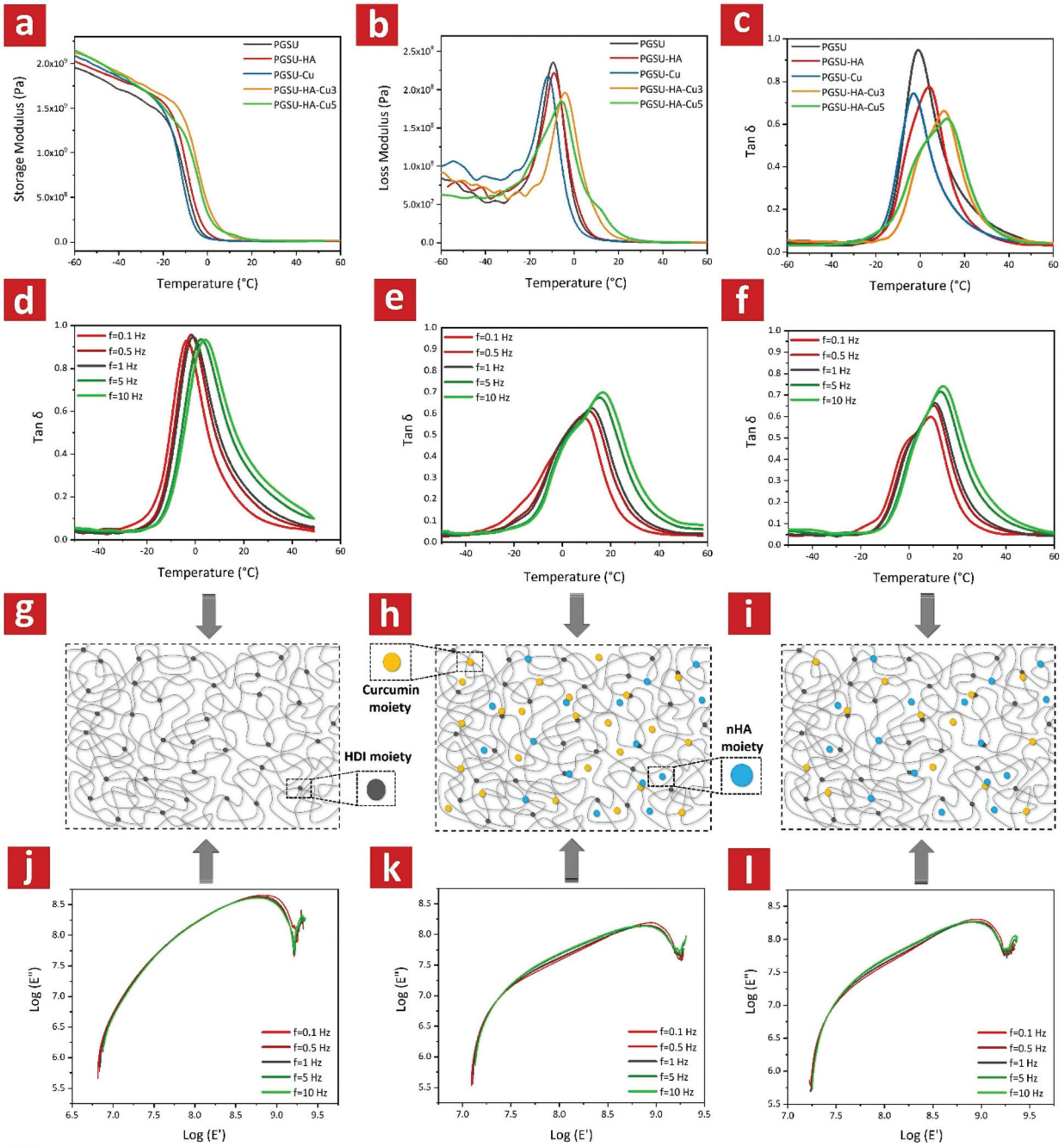

Fig. 6 DMTA analysis of the PGSU-based elastomers: (a) storage modulus, (b) loss modulus and (c) tan(δ). Effect of multi frequencies on loss factor (tan δ) of (d) PGSU, (e) PGSU-HA-Cu5, and (f) PGSU-HA-Cu3. Schematic of the polymer network of (g) PGSU, (h) PGSU-HA-Cu5, and (i) PGSU-Ha-Cu3; by adding the fillers, different networks form and each one puts some restrictions on the mobility of the chains. Cole–Cole plots at various frequencies: (j) PGSU, (k) PGSU-HA-Cu5, and (l) PGSU-HA-Cu3.

Table 3 The glass transition temperature of PGSU-based samples obtained by DMTA. The temperature unit is °C

Parameter	PGSU	PGSU-HA	PGSU-Cu	PGSU-HA-Cu5	PGSU-HA-Cu3
Loss modulus	−9.5	−9	−11.5	−5.5	−4
Tan δ	−1	4	−3	12	10.5

enced the T_g of the PGSU matrix. On the other hand, the hybrid composites exhibit a loss modulus peak which has a maxima at −5.5 °C (PGSU-HA-Cu5) and −4 °C (PGSU-HA-Cu3), noticeably higher than T_g of PGSU. This behavior was expected as the hybrid nanocomposites possess a considerably higher crosslinking density compared to pure PGSU. It is worth mentioning that the glass transition temperature of the hybrid composites increased by reducing the amount of curcumin. This observation can be due to the crosslinking density of PGSU-HA-Cu3 being lower than that of PGSU-HA-Cu5, the lower free volume in the PGSU-HA-Cu3 system (because of less curcumin content and then less fraction of aromaticity in the system) leads to greater reduction in the polymer chain flexibility than in PGSU-HA-Cu5; therefore the free movement among the macromolecular chains would happen at a higher temperature.

Broad tan(δ) peaks obtained for the hybrid composites indicate that these samples are relatively heterogeneous and possess a wide distribution of relaxation times for the PGSU chains due to the formation of a dual filler network originating from the coexistence of curcumin and nHA phases within the network (Fig. 6c). In contrast, other samples exhibited a fairly narrower peak, indicative of a more homogeneous microstructure. By adding nHA, curcumin, or their hybrid compounds, the top of the of tan(δ) peak was reduced, *i.e.*, both curcumin and nHA contributed to increasing rigidity and elastic-like properties in PGSU. The tan(δ) peak of the hybrid composites shows a lower intensity (*i.e.*, lower damping) in comparison with other samples, authenticating the higher degree of crosslinking of the hybrid elastomers.

Fig. 6(d–f) indicates the effect of multi frequency mode on tan(δ) (also, see Fig. S2 in the ESI†). It can be seen that the tan (δ) peak and the corresponding T_g value were shifted to a higher temperature by increasing the frequency. Higher frequency is correlated with less time to respond to an external force or deformation; consequently, more energy (higher temperature) is needed for the polymer macromolecule to trigger the coordinated segmental movement of relaxation.[54] Besides, for all composites, the tan(δ) height and its broadness increased with the increase in frequency, indicative of more heterogeneous behavior of PGSU-based composites at higher frequencies. It is noteworthy that this heterogeneity was more accented in the PGSU-HA-Cu5. Combining two types of fillers leads to forming a separated filler network; consequently, each network will put some restrictions on the mobility of the matrix chains (Fig. 6(g–i)).[18] E' and E'' plots of the investigated samples at different frequencies have also been presented in the ESI (Fig. S3 and S4†).

Fig. 6(j–l) shows the Cole–Cole plots of the samples at different frequencies (also, see Fig. S5†). The non-semicircular curves reveal that the PGSU-based elastomers are heterogeneous. Incorporation of the fillers changed the shape of the PGSU Cole–Cole plot from an almost semicircular curve to a more imperfect semicircular curves, proving that the presence of curcumin and nHA leads to an increase in the heterogeneity of the PGSU network and formation of multiphase systems, which could influence the dynamic mechanical properties of the bioelastomers, as discussed earlier.

The time-temperature superposition (TTS) principle expresses the equivalence between the effects of time and temperature on the viscoelastic behavior of polymers and makes it possible to predict the long-term dynamic mechanical performance of polymers.[53,54] Based on TTS, an increase in temperature at a constant frequency has the same effects in the viscoelastic properties as a decrease in frequency at a constant temperature and *vice versa*. In this work, 37 °C was considered as the reference temperature (T_r) to construct master curves and study the long-term viscoelastic responses of the synthesized bioelastomers at body temperature. For this aim, the glass transition temperatures were chosen based on the loss modulus peak at 1 Hz, and the master curves were constructed through equations (S1)–(S4) (Fig. S6 and Table S1†). Fig. 7 shows the comparison between the master curves of the synthesized bioelastomers. As can be seen, the increasing frequency increased the storage modulus of the samples. From this results can be seen that, the hybrid nanocomposites sample showed higher storage modulus at amplitudes of all frequencies compared to other PGSU-based elastomers, where PGSU-HA-Cu3 exhibited the highest load-bearing properties at low frequencies corresponding to long times (f < 102 Hz), while PGSU showed the lowest storage modulus at low frequencies. One could infer from the obtained master curves that the simultaneous presence of curcumin and nHA can cause robust elastic behavior of the bioelastomers at low frequencies. Therefore the hybrid samples can maintain higher storage modulus and elastic properties than other samples at long times.

3.5. Surface wettability and hydrolytic degradation study

Reaching a desirable biomaterial designed for biomedical purposes to interact with a biological host strongly depends on its surface properties and wettability. Besides, hydrophilicity would noticeably influence the hydrolytic degradation kinetics.[55] Therefore the surface wettability and hydrolytic degradation of the synthesized bioelastomers were determined to assess their potential for biomedical applications. The results of contact angle measurement are shown in Fig. 8(a and b). Fig. 8a exhibits the responses of the bioelastomer surface to an external aqueous environment and the tendency of the samples to interact with water and DMF drops. Since DMF possesses a lower surface tension than water, therefore, it shows considerably lower contact angle in comparison with water drops.[56]

The water contact angle of the PGSU surface was observed to be 85.0 ± 2.2° (Fig. 8b). The addition of nHA significantly enhanced the hydrophilicity of the PGSU matrix and reduced the water contact angle to 71.8± 1.1°. On the other hand, the presence of curcumin in the PGSU network increased hydrophobicity up to about 3° due to the hydrophobic nature of curcumin. Interestingly, the hybrid composites showed higher hydrophilicity than pure PGSU, and water contact angles of 79.9 ± 3.2° and 78.0 ± 2.8° were observed for PGSU-HA-Cu5 and PGSU-HA-Cu3, respectively. One could infer from this

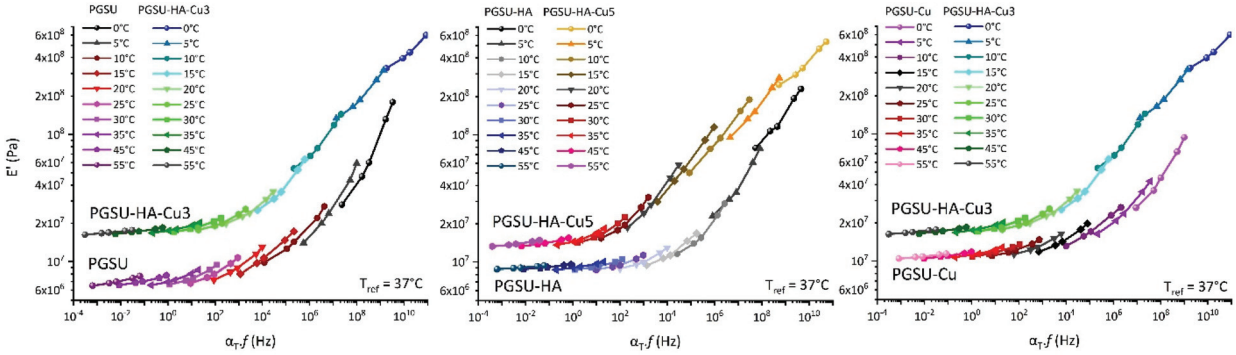

Fig. 7 Comparison between the master curves of the PGSU-based elastomers generated from shifted data at the reference temperature of 37 °C.

observation that compared with curcumin, nHA has a higher impact on the hydrophilic properties of PGSU.

DMF contact angle measurement was performed for a more in-depth investigation of the surface properties and wettability of the PGSU-based bioelastomers (Fig. 8b). Surface free energy values, including polar and the dispersive portions calculated through the Owens–Wendt and Wu methods, are tabulated in Table 4. By adding curcumin, the surface free energy of PGSU reduced from 31.68 to 30.72 mN m^{-1}; consequently, PGSU-Cu showed lower hydrophilicity than pure PGSU. Adding nHA raised the total surface energy and the polar portion of the PGSU matrix, leading to a remarkable increase in the hydrophilic properties. These observations confirm the impact of nHA and curcumin on the changing of surface properties of PGSU. In this work, the surface wettability and hydrophilicity of the samples indicate that the synthesized elastomers could provide favorable conditions for cell adhesion and proliferation, as well as drug loading.

The result of contact angle measurement was further supported by determining the hydration degree of the samples (Fig. 8c). The incorporation of nHA considerably increased the water uptake ability of the PGSU matrix due to the higher hydrophilicity of PGSU-HA than of PGSU although PGSU-HA possesses a higher degree of crosslinking compared to PGSU. Herein, hydrophilicity and crosslinking density are two major factors that determine the water uptake ability of the polymer matrix. For the curcumin-containing samples, both factors seem to be in agreement with each other (high crosslinking degree and low hydrophilicity); hence their swelling degree is lower than that of PGSU and PGSU-HA. It is expected that this may also reduce the degradation rate of the polyester backbone.

Controlled hydrolytic degradation is one of the main goals for new polymers in tissue engineering or controlled delivery applications. Fig. 8d and S7† show the hydrolytic degradation of PGSU and its corresponding composites determined under physiological conditions (lipase enzyme-containing PBS solution, 37 °C). As shown, all the samples display an almost linear degradation profile, which is desirable for tissue-engineered scaffolds to follow.[20] The mass loss for PGSU after 30 days was 21.5 ± 1.3% (degradation rate of ~5% per week). The addition of nHA resulted in an accelerated degradation with mass loss (*i.e.*, degradation rate) of 23.5 ± 1.3% (~5% per week) and reduced physiological stability of the PGSU, as was expected from the results of contact angle measurement and water uptake capacity. Meanwhile, the addition of curcumin showed no noticeable influence on PGSU degradation (mass loss of 20.5 ± 1.5% and degradation rate of ~4.8% per week). Although PGSU-Cu shows a higher hydrophobicity and crosslinking density than PGSU, at least a part of the mass loss of PGSU-Cu can possibly be attributed to its noticeable release rate of curcumin during hydrolytic degradation (discussed later in the section "Curcumin release test"), which probably allows more water molecules to diffuse into the PGSU network and access hydrolytically labile bonds by time and alleviate the impact of hydrophilicity and degree of crosslinking on the degradation of PGSU-Cu. On the other hand, simultaneously incorporating curcumin and nHA retarded the degradation of the PGSU network, where PGSU-HA-Cu5 and PGSU-HA-Cu3 exhibited mass loss of 14.9 ± 1.2% (~3.5% per week) and 17.85 ± 1.2% (~4.2% per week), respectively. The higher physiological stability of the hybrid elastomers could be due to the fact that the hybrid samples possess a substantially higher degree of crosslinking (Table 2) and lower hydrophilicity and water uptake ability (Fig. 8(a–c)) than PGSU.

Furthermore, the surfaces of the bioelastomers before and after hydrolytic degradation for 30 days were compared using SEM images (Fig. 8e). Surface erosion is known as the main degradation mechanism for PGS[20] and PGSU.[48] Surfaces of PGSU-HA-Cu5 and PGSU-HA-Cu3 kept almost smooth during 30 days of degradation. However, the surfaces of the other samples showed obvious signs of surface degradation, characterized by rough surfaces and irregular pits. The results of SEM could also approve the difference in the degradation rate of the samples. The higher hydrophilicity and water uptake ability of PGSU-HA would facilitate water molecule penetration into the polymeric network; consequently, a higher surface area would be exposed to the aqueous environment, leading to a higher rate of the PGSU matrix hydrolysis and degradation. On the other hand, despite the higher degree of crosslinking and lower hydrophilicity and swelling degree of PGSU-Cu than PGSU and PGSU-HA, dissolution and diffusion of curcumin

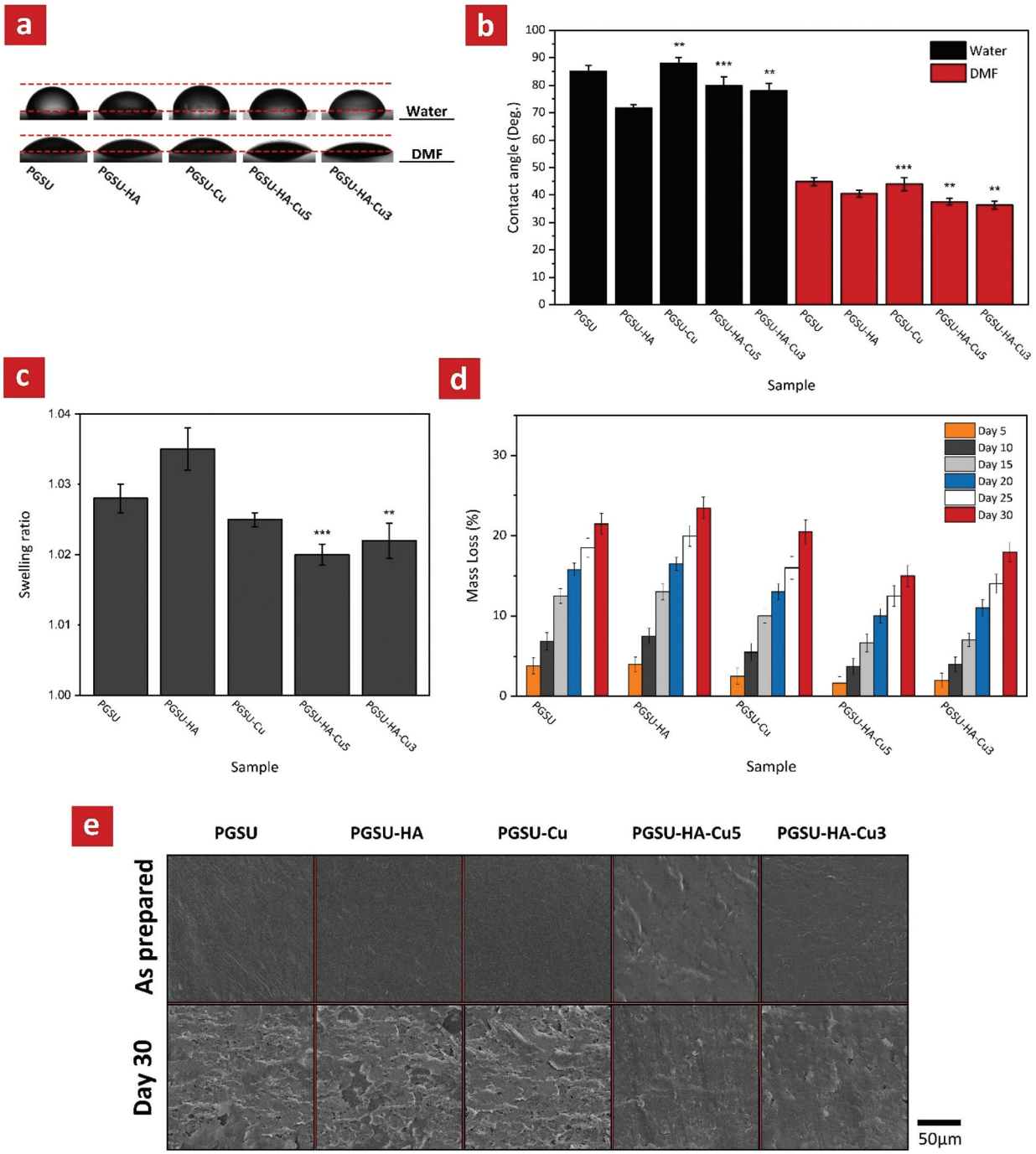

Fig. 8 (a) Images of contact angle measurement and drop shape analysis. (b) Water and DMF contact angles of the synthesized bioelastomers. (c) Swelling behavior and water uptake ability at 37 °C. (d) *In vitro* enzymatic degradation profile of the bioelastomers in PBS solution (pH = 7.4) at 37 °C. (e) SEM images of the surface of the samples before and after 30 days of hydrolytic degradation. (Statistical significance was shown as $*p < 0.05$, $**p < 0.01$, $***p < 0.001$, $n = 3$).

into the PBS solution can also facilitate the degradation of PGSU-Cu. Such a hydrolytic degradation range accompanied by favorable hydrophilicity properties allows achieving a desirable balance of degradation kinetics and mechanical flexibility simultaneously in order to design various biomimetic scaffolds with tunable properties.

3.6. Protein adsorption, curcumin release test and antibacterial activity

Protein adsorption highly depends on the surface composition of biomaterials and is the first process that takes place upon implantation of a scaffold in the human body.[57] To further

Table 4 Water and DMF contact angle and free surface energy of the synthesized elastomers

			Wu method			Owens–Wendt method		
Sample	Water contact angle (°)	DMF contact angle (°)	Total surface energy (mN m^{-1})	Disperse part (mN m^{-1})	Polar part (mN m^{-1})	Total surface energy (mN m^{-1})	Disperse part (mN m^{-1})	Polar part (mN m^{-1})
PGSU	85.0	44.9	31.68	20.38	11.30	27.7	21.35	6.35
PGSU-HA	71.8	40.5	38.51	20.53	17.98	33.36	18.07	15.29
PGSU-Cu	88.1	43.9	30.72	21.15	9.57	27.67	23.18	4.49
PGSU-HA-Cu5	79.9	37.5	35.20	22.15	13.05	30.95	22.67	8.28
PGSU-HA-Cu3	78.0	36.2	36.26	22.34	13.92	31.78	22.40	9.38

assess the effect of nHA and curcumin on the surface properties of the bioelastomers, protein adsorption was studied (Fig. 9a). Proteins adsorbed on the scaffold surfaces could significantly affect cell–biomaterial interactions. The result reveals that the protein adsorbed on the surface of the bioelastomers was about twofold more than TCPS control. Adding nHA enhanced the protein adsorption, while the introduction of the curcumin to the PGSU matrix had no noticeable effects on protein adsorption. Higher protein adsorption of PGSU-HA could be due to the presence of Ca^{2+} and PO_4^{3-} of nHA on the

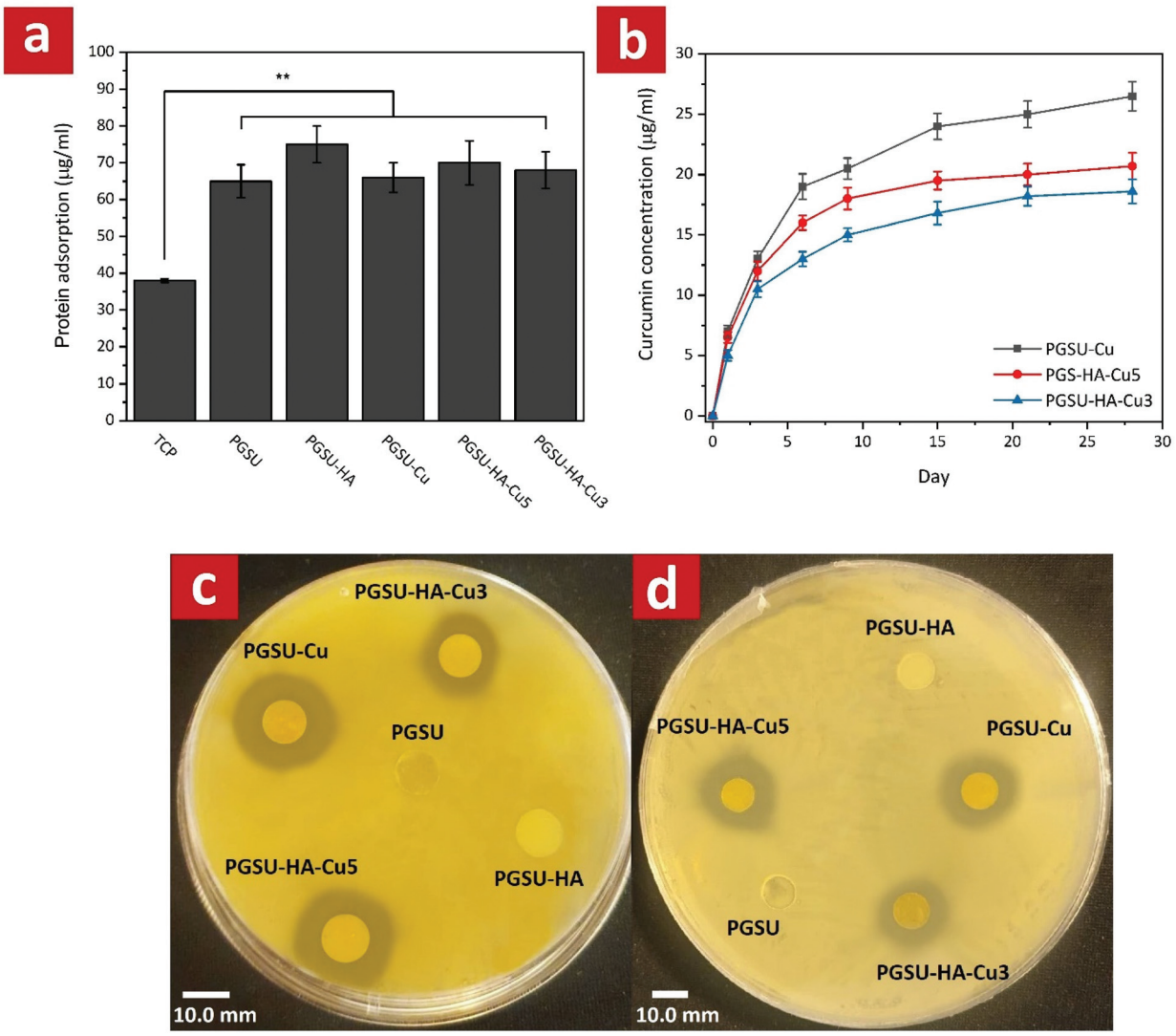

Fig. 9 (a) Protein adsorption on the surface of the synthesized bioelastomers. (b) Curcumin release of the curcumin-containing elastomers in PBS (PH 7.4, 37 °C) during hydrolytic degradation. Antibacterial activity of PGSU-based elastomers against (c) *P. aeruginosa* and (d) *S. aureus*. (Statistical significance was shown as $*p < 0.05$, $**p < 0.01$, $***p < 0.001$, $n = 3$).

polymer surface, which can act as the protein binding sites and provide a significant driving force for protein adsorption.[58]

The drug release trend of an implanted bioelastomer scaffold could noticeably be affected by its crosslinking degree, hydrophilicity, and degradation rate. The release profile of curcumin-loaded samples (Fig. 9b) reveals a relatively rapid release, where most of the curcumin elution happens within a timeframe of 9 days, followed by sustained release up to day 28. The faster curcumin release rate at the early releasing stage (before day 9) could be attributed to the physically bonded curcumin in the PGSU matrix, which can much easily dissolve and diffuse at the early degradation period in comparison with the chemically bonded curcumin. The highest curcumin release was observed in PGSU-Cu due to its lower degree of crosslinking, faster degradation rate, and higher water uptake ability than the hybrid samples. Among the hybrid bioelastomers, PGSU-HA-Cu5 shows a higher release rate than PGSU-HA-Cu3. Despite the higher degree of crosslinking as well as lower degradation rate and water uptake ability of PGSU-HA-Cu5 compared to PGSU-HA-Cu3, higher curcumin content in PGSU-HA-Cu5 imparts higher physically entrapped curcumin in the polymer network, allowing much more curcumin releasing during the hydrolytic degradation process.

Antibacterial activity of the synthesized elastomers was evaluated by measuring the zone of inhibition against two bacterial strains (Fig. 9(c and d)). *P. aeruginosa* (Gram −) and *S. aureus* (Gram +) were chosen as model bacteria, and the inhibition zone diameter data are tabulated in Table 5. Clearly, PGSU and PGSU-nHA did not show antibacterial activity. In comparison, the samples containing curcumin showed a substantial antibacterial effect. Microbiological results show that the presence of curcumin had a desirable inhibitory effect against both bacteria, *i.e.*, curcumin acceptably hindered the *P. aeruginosa* and *S. aureus* cell growth. It is suggested that the antimicrobial activity of curcumin is due to membrane damage and bacterial cell lysis by the binding of curcumin and peptidoglycan layer on the cell wall of Gram-positive and Gram-negative bacteria; also, curcumin can bind into FtsZ proteins, and hinder the FtsZ protofilament assembly, thereby hindering cell migration and bacterial proliferation and finally causing bacterial cell death.[59,60]

3.7. *In vitro* biocompatibility and cell culture experiments

In tissue engineering, implanted scaffolds in the human body must provide a viable environment for the cells to induce their adherence and proliferation. After evaluating the properties of the bioelastomers synthesized in this study, PGSU-HA and PGSU-HA-Cu5 were selected as representatives to assess *in vitro* biocompatibility and cell viability. Although biocompatibility of PGSU elastomers has been proved before,[48] to study the biocompatibility of the PGSU nanocomposites comparatively, cell viability of the PGSU sample was also evaluated in this work. The viability of L929 cells on the bioelastomer surface was investigated by MTT assay at predetermined time intervals of cultivation (1, 3, 5, and 7 days). Fig. 10a exhibits a continuous increase in the number of viable cells on the surface of the sample with culture time. In comparison with the TCPS control, the viability activity of seeded L929 cells on PGSU surfaces was almost half that of the TCPS. As expected, a significant difference in the metabolic activity of cultured L929 cells was observed due to the addition of nHA and curcumin. While fewer cells were attached to PGSU-HA and PGSU-HA-Cu5 than to TCPS (day 1), cells proliferated on both PGSU-HA and PGSU-HA-Cu5 and on day 7 they showed the number of cells almost equal to that of TCPS.

The proliferation kinetics study (Fig. 10b) showed that the cell growth in both PGSU-HA and PGSU-HA-Cu5 increased in an almost similar and linear rate up to day 5, where their cell proliferation rate was boosted after day 5 of cell cultivation. To summarize, the MTT assay study indicated that the addition of nHA and curcumin could be beneficial to the proliferation of L929 mouse fibroblast cells.

To further evaluate the cell–matrix interactions and the scaffold bioactivity, SEM images were taken from the surface of the polymer after 3 days of cell culture (Fig. 10c). As shown, normal morphology and shape for mouse fibroblast cells can be seen on day 3. Moreover, both the substrates supported cell adherence. Favorable cell spreading and attachment on the bioelastomer surface were observed, indicating the feasibility of the synthesized bioelastomers for tissue engineering applications. The result of MTT assay and cell culture morphology was further supported by data of DAPI staining of the cell nuclei (Fig. 10d), where the fluorescence images showed almost analogous cell attachment and proliferation for PGSU-HA and PGSU-HA-Cu5 at days 1 and 5 after cell cultivation.

The bioelastomer bioactivity can be highly influenced by their degradation rate, hydrophilicity, and swelling behavior. Cellular metabolic, cell viability, and proliferative activities can be stimulated by a slower degradation rate; PGS hydrolysis during the degradation process provides an acidic environment by reducing the local pH, which is undesirable for cell adherence and proliferation.[23,24,61] From this point of view, PGSU-HA-Cu5 can present better cell viability than PGSU and PGSU-HA. On the other hand, high hydrophilicity and swelling in aqueous media can also play a significant role in cell metabolic activity, which can convert into higher cell viability of PGSU-HA in comparison with PGSU and PGSU-HA-Cu5. After

Table 5 Diameter of inhibition zone of the PGSU-based films

	Bacteria	PGSU	PGSU-HA	PGSU-Cu	PGSU-HA-Cu5	PGSU-HA-Cu3
Diameter (mm)	*P. aeruginosa*	0	0	24.2 ± 1.9	23.6 ± 0.5	19.2 ± 0.8
	S. aureus	0	0	22.6 ± 0.3	20.6±.9	18.0 ± 0.7

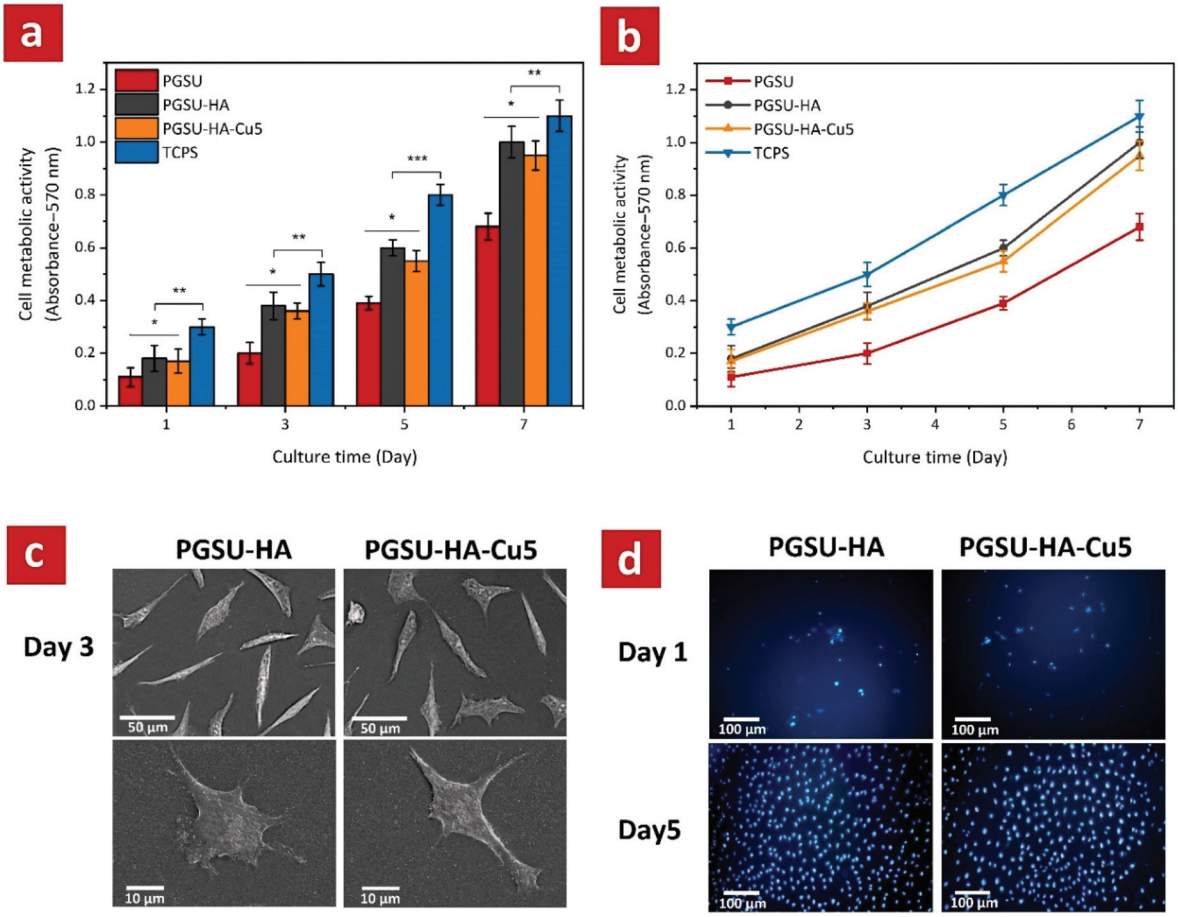

Fig. 10 *In vitro* biocompatibility study of the PGSU-based elastomers. (a) Cell viability measured by MTT assay. TCPS surface was used as positive control. (b) Proliferation kinetics of L929 mouse fibroblast cells on the bioelastomer film and on TCPS, evaluated using MTT assay. (c) Comparison of L929 mouse fibroblast cell morphology when seeded on PGSU-HA and PGSU-HA-Cu5 at day 3. (d) DAPI staining of L929 cells on the bioelastomers at days 1 and 5. (Statistical significance was shown as $*p < 0.05$, $**p < 0.01$, $***p < 0.001$, $n = 3$).

all, biocompatibility and non-toxicity of nano-hydroxyapatite[29] and curcumin[34,40,43] can also enhance cell viability and proliferation.

The results of cell metabolic activity indicated that biomimetic PGSU-based elastomers promote cell spreading and proliferation, suggesting that the addition of curcumin and nHA can enhance the physiological performance and bioactivity of the PGSU scaffolds, and making them desirable for tissue engineering applications. However, further *in vivo* studies are needed to evaluate the long-term efficacy of the bioelastomers synthesized in this study.

4. Conclusion

By incorporating hydroxyapatite nanoparticles and curcumin within PGSU, we achieved novel biomedical scaffolds that could be applied for various biomedicine purposes such as regenerative medicine as well as for a range of biomedical tissues. In this regard, different PGSU-based elastomers were successfully synthesized with different concentrations of nHA and curcumin and using hexamethylene diisocyanate (HDI) as a crosslinker. FTIR analyses showed that PGSU-based elastomers had been synthesized correctly. The morphology of the samples was evaluated by SEM and EDX, in which the proper dispersion of hydroxyapatite nanoparticles, particularly in the presence of curcumin, was demonstrated. The Young's modulus, ultimate tensile strength, and compression modulus of the bioelastomers were improved with the presence of nHA and curcumin in the polymeric network, allowing us to design scaffolds with acceptable mechanical range used in hard tissue engineering. DMAT analyses indicated that nHA and curcumin alter the PGSU structure by changing T_g and viscoelastic properties. The contact angle measurement showed that hydrophilic behavior and surface wettability were influenced noticeably by adding nHA. Furthermore, while nHA accelerated hydrolytic degradation of PGSU, nHA/curcumin hybrid compounds significantly retarded it. We also found that the elastomers containing curcumin have a noticeable antibacterial effect against *P. aeruginosa* and *S. aureus* strains.

The culture of L929 cells on the surface of the nanocomposites indicated high cell viability and improved proliferation and metabolic activity, showing the biocompatibility of the synthesized bioelastomers. Overall, the results obtained in this study introduce PGSU composites as promising candidates and potential platforms for various tissue engineering applications, specifically hard tissues. Such applications require multifunctional properties, including good cell viability and metabolic activity, suitable mechanical properties, antimicrobial activity, favorable hydrophilicity, and degradation rate, which were demonstrated in the reported bioelastomers. In future studies, we will focus on validating the *in vivo* implantability and osteoinductive potential of the engineered bioelastomers.

Conflicts of interest

There are no conflicts to declare.

References

1 J. M. Kanczler, J. A. Wells, D. M. R. Gibbs, K. M. Marshall, D. K. O. Tang and R. O. C. Oreffo, in *Principles of Tissue Engineering*, ed. R. Lanza, R. Langer, J. P. Vacanti and A. Atala, Academic Press, 5th edn, 2020, pp. 917–935. DOI: 10.1016/B978-0-12-818422-6.00052-6.
2 S. Ullah and X. Chen, *Appl. Mater. Today*, 2020, **20**, 100656.
3 L.-Q. Yang, B. He, S. Meng, J.-Z. Zhang, M. Li, J. Guo, Y.-M. Guan, J.-X. Li and Z.-W. Gu, *Polymer*, 2013, **54**, 2668–2675.
4 S. Chen, X. Bi, L. Sun, J. Gao, P. Huang, X. Fan, Z. You and Y. Wang, *ACS Appl. Mater. Interfaces*, 2016, **8**, 20591–20599.
5 H. Daemi, S. Rajabi-Zeleti, H. Sardon, M. Barikani, A. Khademhosseini, A. Khademhosseini and H. Baharvand, *Biomaterials*, 2016, **84**, 54–63.
6 F. Hosseini Chenani, V. F. Rezaei, V. Fakhri, F. R. Wurm, L. Uzun and V. Goodarzi, *J. Appl. Polym. Sci.*, 2021, **138**, 50563.
7 J. Hu, D. Kai, H. Ye, L. Tian, X. Ding, S. Ramakrishna and X. J. Loh, *Mater. Sci. Eng., C*, 2017, **70**, 1089–1094.
8 J. M. Kemppainen and S. J. Hollister, *J. Biomed. Mater. Res., Part A*, 2010, **94A**, 9–18.
9 X. Zhang, C. Jia, X. Qiao, T. Liu and K. Sun, *Polym. Test.*, 2016, **54**, 118–125.
10 K. Yang, J. Zhang, X. Ma, Y. Ma, C. Kan, H. Ma, Y. Li, Y. Yuan and C. Liu, *Mater. Sci. Eng., C*, 2015, **56**, 37–47.
11 T. H. Qazi, R. Rai, D. Dippold, J. E. Roether, D. W. Schubert, E. Rosellini, N. Barbani and A. R. Boccaccini, *Acta Biomater.*, 2014, **10**, 2434–2445.
12 Q.-Z. Chen, A. Bismarck, U. Hansen, S. Junaid, M. Q. Tran, S. E. Harding, N. N. Ali and A. R. Boccaccini, *Biomaterials*, 2008, **29**, 47–57.
13 I. Pomerantseva, N. Krebs, A. Hart, C. M. Neville, A. Y. Huang and C. A. Sundback, *J. Biomed. Mater. Res., Part A*, 2009, **91**, 1038–1047.
14 X. J. Loh, A. Abdul Karim and C. Owh, *J. Mater. Chem. B*, 2015, **3**, 7641–7652.
15 Y. Wang, G. A. Ameer, B. J. Sheppard and R. Langer, *Nat. Biotechnol.*, 2002, **20**, 602–606.
16 Z. Wang, Y. Ma, Y. Wang, Y. Liu, K. Chen, Z. Wu, S. Yu, Y. Yuan and C. Liu, *Acta Biomater.*, 2018, **71**, 279–292.
17 X. Zhao, Y. Wu, Y. Du, X. Chen, B. Lei, Y. Xue and P. X. Ma, *J. Mater. Chem. B*, 2015, **3**, 3222–3233.
18 M. H. Aghajan, M. Panahi-Sarmad, N. Alikarami, S. Shojaei, A. Saeidi, H. A. Khonakdar, M. Shahrousvan and V. Goodarzi, *Eur. Polym. J.*, 2020, **131**, 109720.
19 M. Rostamian, M. R. Kalaee, S. R. Dehkordi, M. Panahi-Sarmad, M. Tirgar and V. Goodarzi, *Eur. Polym. J.*, 2020, **138**, 109985.
20 A. K. Gaharwar, A. Patel, A. Dolatshahi-Pirouz, H. Zhang, K. Rangarajan, G. Iviglia, S.-R. Shin, M. A. Hussain and A. Khademhosseini, *Biomater. Sci.*, 2015, **3**, 46–58.
21 M. Frydrych, S. Román, S. MacNeil and B. Chen, *Acta Biomater.*, 2015, **18**, 40–49.
22 Q.-Z. Chen, S.-L. Liang, J. Wang and G. P. Simon, *J. Mech. Behav. Biomed. Mater.*, 2011, **4**, 1805–1818.
23 S.-L. Liang, W. D. Cook, G. A. Thouas and Q.-Z. Chen, *Biomaterials*, 2010, **31**, 8516–8529.
24 C. C. Lau, M. Al Qaysi, N. Owji, M. K. Bayazit, J. Xie, J. C. Knowles and J. Tang, *Mater. Today Adv.*, 2020, **5**, 100023.
25 M. Frydrych, S. Román, N. H. Green, S. MacNeil and B. Chen, *Polym. Chem.*, 2015, **6**, 7974–7987.
26 M. Frydrych and B. Chen, *Polymer*, 2017, **122**, 159–168.
27 T. Wu, M. Frydrych, K. O'Kelly and B. Chen, *Biomacromolecules*, 2014, **15**, 2663–2671.
28 G. E. Poinern, R. K. Brundavanam, N. Mondinos and Z.-T. Jiang, *Ultrason. Sonochem.*, 2009, **16**, 469–474.
29 H. Zhou and J. Lee, *Acta Biomater.*, 2011, **7**, 2769–2781.
30 S. M. Zakaria, S. H. Sharif Zein, M. R. Othman, F. Yang and J. A. Jansen, *Tissue Eng., Part B*, 2013, **19**, 431–441.
31 J. Venkatesan and S.-K. Kim, *J. Biomed. Nanotechnol.*, 2014, **10**, 3124–3140.
32 K. Pielichowska, K. Król and T. M. Majka, *Thermochim. Acta*, 2016, **633**, 98–107.
33 M. Szlachta, K. Ordon, K. Nowicka and K. Pielichowska, *J. Therm. Anal. Calorim.*, 2021, **143**, 3471–3478.
34 D. Akbik, M. Ghadiri, W. Chrzanowski and R. Rohanizadeh, *Life Sci.*, 2014, **116**, 1–7.
35 P. B. Tsekova, M. G. Spasova, N. E. Manolova, N. D. Markova and I. B. Rashkov, *Mater. Sci. Eng., C*, 2017, **73**, 206–214.
36 D. Praditya, L. Kirchhoff, J. Brüning, H. Rachmawati, J. Steinmann and E. Steinmann, *Front. Microbiol.*, 2019, **10**, 912.
37 Bhawana, R. K. Basniwal, H. S. Buttar, V. K. Jain and N. Jain, *J. Agric. Food Chem.*, 2011, **59**, 2056–2061.
38 B. B. Aggarwal and B. Sung, *Trends Pharmacol. Sci.*, 2009, **30**, 85–94.

39 S. Oprea, V. O. Potolinca and V. Oprea, *J. Polym. Res.*, 2020, **27**, 60.
40 X. Li, K. Nan, L. Li, Z. Zhang and H. Chen, *Carbohydr. Polym.*, 2012, **88**, 84–90.
41 M. F. Abdollahi, M. Zandi, P. Shokrollahi and M. Ehsani, *J. Polym. Res.*, 2015, **22**, 179.
42 K. Mahmood, K. M. Zia, W. Aftab, M. Zuber, S. Tabasum, A. Noreen and F. Zia, *Int. J. Biol. Macromol.*, 2018, **113**, 150–158.
43 Z.-J. Sun, B. Sun, R.-B. Tao, X. Xie, X.-L. Lu and D.-L. Dong, *J. Biomed. Mater. Res., Part A*, 2013, **101A**, 253–260.
44 V. Fakhri, M. Monem, G. Mir Mohamad Sadeghi, H. A. Khonakdar, V. Goodarzi and N. Karimpour-Motlagh, *Polym. Adv. Technol.*, 2021, DOI: 10.1002/pat.5444.
45 F. Tang, G. Xu, T. Ma and L. Kong, *Materials*, 2018, **11**(9), 1488.
46 Z. Song, W. Zhu, N. Liu, F. Yang and R. Feng, *Int. J. Pharm.*, 2014, **471**, 312–321.
47 T. Zhang, W. Cai, F. Chu, F. Zhou, S. Liang, C. Ma and Y. Hu, *Composites, Part A*, 2020, **128**, 105681.
48 M. J. N. Pereira, B. Ouyang, C. A. Sundback, N. Lang, I. Friehs, S. Mureli, I. Pomerantseva, J. McFadden, M. C. Mochel, O. Mwizerwa, P. del Nido, D. Sarkar, P. T. Masiakos, R. Langer, L. S. Ferreira and J. M. Karp, *Adv. Mater.*, 2013, **25**, 1209–1215.
49 Y. Yan, V. Sencadas, T. Jin, X. Huang, W. Lie, D. Wei and Z. Jiang, *J. Colloid Interface Sci.*, 2018, **521**, 24–32.
50 Y. Yan, M. Potts, Z. Jiang and V. Sencadas, *Compos. Sci. Technol.*, 2018, **162**, 14–22.
51 T. Zhang, W. Cai, F. Chu, F. Zhou, S. Liang, C. Ma and Y. Hu, *Composites, Part A*, 2020, **128**, 105681.
52 B. Lowe, J. G. Hardy and L. J. Walsh, *ACS Omega*, 2020, **5**, 1–9.
53 R. F. Landel and L. E. Nielsen, *Mechanical Properties of Polymers and Composites*, CRC Press, 1993.
54 D. Ionita, M. Cristea and C. Gaina, *Polym. Test.*, 2020, **83**, 106340.
55 L. N. Woodard and M. A. Grunlan, *ACS Macro Lett.*, 2018, **7**, 976–982.
56 M. I. Jamil, L. Song, J. Zhu, N. Ahmed, X. Zhan, F. Chen, D. Cheng and Q. Zhang, *RSC Adv.*, 2020, **10**, 19157–19168.
57 H. P. Felgueiras, J. C. Antunes, M. C. L. Martins and M. A. Barbosa, in *Peptides and Proteins as Biomaterials for Tissue Regeneration and Repair*, ed. M. A. Barbosa and M. C. L. Martins, Woodhead Publishing, 2018, pp. 1–27. DOI: 10.1016/B978-0-08-100803-4.00001-2.
58 K. Wang, C. Zhou, Y. Hong and X. Zhang, *Interfaces Focus*, 2012, **2**(3), 259–277.
59 S. Roy and J.-W. Rhim, *Int. J. Biol. Macromol.*, 2020, **162**, 1780–1789.
60 S.-Y. Teow, K. Liew, S. A. Ali, A. S.-B. Khoo and S.-C. Peh, *J. Trop. Med.*, 2016, **2016**, 2853045.
61 P. Kerativitayanan and A. K. Gaharwar, *Acta Biomater.*, 2015, **26**, 34–44.

